Free Radical Reactions Involving Cl•, Cl2−•, and SO4−• in the 248 nm Photolysis of Aqueous Solutions Containing S2O82− and Cl−

ARTICLE *in* THE JOURNAL OF PHYSICAL CHEMISTRY A · DECEMBER 2003

Impact Factor: 2.69 · DOI: 10.1021/jp036211i

3 AUTHORS, INCLUDING:

Xiao-Ying Yu
Pacific Northwest National Laboratory
82 PUBLICATIONS **1,009** CITATIONS
SEE PROFILE

John R. Barker
University of Michigan
171 PUBLICATIONS **5,939** CITATIONS
SEE PROFILE

Free Radical Reactions Involving $Cl^{\bullet}$, $Cl_2^{-\bullet}$, and $SO_4^{-\bullet}$ in the 248 nm Photolysis of Aqueous Solutions Containing $S_2O_8^{2-}$ and Cl^-

Xiao-Ying Yu,[†,‡] Zhen-Chuan Bao,[§,⊥] and John R. Barker*[,†,§]

Department of Chemistry, The University of Michigan, Ann Arbor, Michigan 48109-1055, and Department of Atmospheric, Oceanic, and Space Sciences, The University of Michigan, Ann Arbor, Michigan 48109-2143

Received: July 29, 2003; In Final Form: October 30, 2003

Rate constants and other properties are reported for photochemical reactions initiated by laser photolysis (248 nm) of $S_2O_8^{2-}$(aq) in acidic solutions containing Cl^-(aq) at 297 ± 2 K. The absorption spectra of $SO_4^{-\bullet}$(aq) and $Cl_2^{-\bullet}$(aq) are measured and compared to literature values. Equilibrium constants and rate constants involving $Cl^{\bullet}$(aq), $Cl_2^{-\bullet}$(aq), H_2O, $SO_4^{-\bullet}$(aq), and $S_2O_8^{2-}$(aq) are determined by analyzing the formation and decay of $Cl_2^{-\bullet}$(aq) and $SO_4^{-\bullet}$(aq) in a self-consistent chemical mechanism. For the first time, the anticipated pH dependence is observed unambiguously in the pseudo-first-order decay rate constant of $Cl_2^{-\bullet}$. The rate constants for the reactions $Cl^{\bullet}(aq) + Cl_2^{-\bullet}(aq) \rightarrow Cl_2(aq) + Cl^-(aq)$ and $Cl_2^{-\bullet}(aq) + Cl_2^{-\bullet}(aq) \rightarrow Cl_2(aq) + 2Cl^-(aq)$ are determined; rate constants for the latter are measured as a function of temperature and ionic strength. In addition, the ionic strength dependence of the reaction $SO_4^{-\bullet}(aq) + Cl^-(aq) \rightarrow SO_4^{2-}(aq) + Cl^{\bullet}(aq)$ is reported. Rate constants for the reactions of $Cl^{\bullet}$(aq) and $Cl_2^{-\bullet}$(aq) with $S_2O_8^{2-}$(aq) are reported for the first time. The present and previous (when available) experimental results are generally in good agreement within the context of the comprehensive chemical mechanism for this system.

1. Introduction

Cloud-, fog-, and rainwater are known to scavenge soluble species from the gas phase in the atmosphere.[1−5] The dissolved species can become highly concentrated when water from the droplet evaporates. Subsequent chemical reactions in the droplet are sometimes orders of magnitude faster than those in the gas phase[6] and can have an important impact on atmospheric chemical processes.[1,2,5−8]

Sea salt is a major source of dissolved halide ions in atmospheric water droplets. In aqueous solution, chloride ions react rapidly with dissolved free radicals such as $OH^{\bullet}$, $NO_3^{\bullet}$, $Cl^{\bullet}$, and $SO_4^{-\bullet}$. (To simplify notation, the "aq" designation on chemical species is omitted in the remainder of this paper.) The present work (designated as Paper III) is one of a series of papers describing the chemical mechanism and kinetics of $Cl^{\bullet}$ and $Cl_2^{-\bullet}$ (dichloride or dichlorine radical anion) in the aqueous phase. Paper I[9] focuses on the chemical mechanism of hydrogen peroxide photolysis of acidic solutions containing chloride ions. Paper II[10] extends the knowledge of the chemical mechanism and reports the primary quantum yield for production of hydroxyl radicals in the photolysis of hydrogen peroxide, as measured using chloride ions as a scavenger. Paper III (this work) deals with the chemical mechanism of $Cl_2^{-\bullet}$ and $SO_4^{-\bullet}$ formation and decay. Paper IV[11] reports evaluations of some of the important rate constants involved in the $Cl_2^{-\bullet}$ formation and decay. The chemical mechanism and rate constants are summarized in Table 1. This mechanism is similar to the ones found for the bromide[12] and iodide systems.[13]

Sulfate radicals ($SO_4^{-\bullet}$) are strong oxidants that react with many species in aqueous systems. They are important precursor radicals in the laboratory and important intermediate species in the autoxidation of S(IV) to S(VI).[1] Sulfate radicals also oxidize chloride ions (Cl^-) to chlorine atoms ($Cl^{\bullet}$). Both $SO_4^{-\bullet}$ and $Cl_2^{-\bullet}$ are of interest in the study of nitrate free radical chemistry, because they are produced in cloudwater by dissolved $NO_3^{\bullet}$ radicals in reactions with other dissolved species.[3] Free radical reactions are important in the inorganic aerosol or raindrop chemistry of nitrogen, sulfur, and the halogens.

The reaction between sulfate radicals and chloride ions rapidly produces solvated chlorine atoms.[14−24] Once chlorine atoms are formed, they quickly react with chloride ions and form an equilibrium with $Cl_2^{-\bullet}$, which absorbs strongly in the ultraviolet. The bimolecular reaction between two $Cl_2^{-\bullet}$ radicals produces Cl_2, which can be released as a gas in the atmosphere. The photochemical reaction mechanism is shown schematically in Figure 1. The goal of our research is to determine the comprehensive reaction mechanism and rate constants in a self-consistent system.

In laboratory studies, persulfate ions ($S_2O_8^{2-}$) are often used as a photochemical precursor for producing sulfate free radicals ($SO_4^{-\bullet}$) in solutions. The thermal, photochemical, and radiation-induced decomposition of potassium persulfate has been studied extensively.[25−32] The structure of the persulfate ion[33] suggests that it consists of two $SO_4^{-\bullet}$ tetrahedra held together by a single homopolar bond between oxygen atoms at one corner of each of the two tetrahedra. Photolysis of $S_2O_8^{2-}$ produces two $SO_4^{-\bullet}$ radicals via a simple O−O bond scission.[29,31] The quantum efficiency of the photodissociation of persulfate ion has been found to be unity for acidic,[27] neutral, and alkaline solutions.[26]

* To whom correspondence should be addressed. E-mail: jrbarker@umich.edu.

† Department of Chemistry.

‡ Present Address: Cloud Simulation and Aerosol Laboratory, Department of Atmospheric Science, Colorado State University, Fort Collins, Colorado 80523-1371.

§ Department of Atmospheric, Oceanic, and Space Sciences.

⊥ Present Address: 22692 Liberty Oak Lane, Cupertino, California 95014.

10.1021/jp036211i CCC: $27.50
Published on Web 12/16/2003

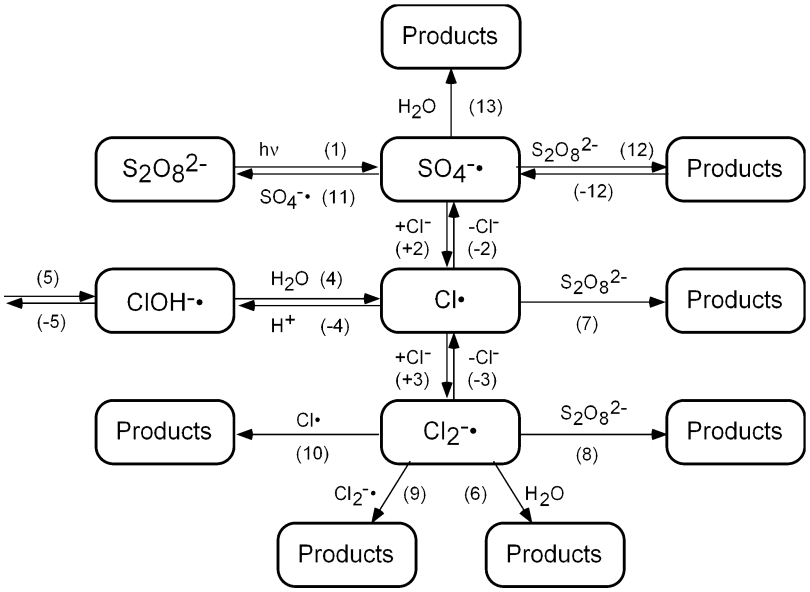

Figure 1. A schematic diagram of the reaction mechanism of $S_2O_8^{2-}$ and Cl^- in the aqueous phase. Reaction numbers (from Table 1) are given in parentheses.

TABLE 1: The Chemical Mechanism of $S_2O_8^{2-}$ and Cl^- in the Aqueous Phase

	reaction	k_f	k_r
1	$S_2O_8^{2-} + h\nu \rightarrow SO_4^{-\bullet} + SO_4^{-\bullet}$	$\Phi_{SO_4^{-\bullet}} = 2$ [32,37,50,92]	
2	$SO_4^{-\bullet} + Cl^- \leftrightarrow SO_4^{2-} + Cl^\bullet$	$k_2 = (3.2 \pm 0.2) \times 10^8\ M^{-1}\ s^{-1}$ [a]	$k_{-2} = (2.1 \pm 0.1) \times 10^8\ M^{-1}\ s^{-1}$ [24]
3	$Cl^\bullet + Cl^- \leftrightarrow Cl_2^{-\bullet}$	$k_3 = (7.8 \pm 0.8) \times 10^9\ M^{-1}\ s^{-1}$ [9] $K_3 = (1.4 \pm 0.2) \times 10^5\ M^{-1}$ [9]	$k_{-3} = (5.7 \pm 0.4) \times 10^4\ s^{-1}$ [9]
4	$Cl^\bullet + H_2O \leftrightarrow ClOH^{-\bullet} + H^+$	$k_4[H_2O] = (1.6 \pm 0.2) \times 10^5\ s^{-1}$ [a] $1/K_4 = (7.2 \pm 1.6) \times 10^6$ [a]	$k_{-4} = (2.6 \pm 0.6) \times 10^{10}\ M^{-1}\ s^{-1}$ [9]
5	$ClOH^{-\bullet} \leftrightarrow HO^\bullet + Cl^-$	$k_5 = (6.1 \pm 0.8) \times 10^9\ s^{-1}$ [16] $1/K_5 = 0.70 \pm 0.13\ M^{-1}$ [16]	$k_{-5} = (4.3 \pm 0.4) \times 10^9\ M^{-1}\ s^{-1}$ [16]
6	$Cl_2^{-\bullet} + H_2O \rightarrow ClOH^{-\bullet} + H^+ + Cl^-$	$k_6[H_2O] < 100\ s^{-1}$ [a,9]	
7	$Cl^\bullet + S_2O_8^{2-} \rightarrow$ products	$k_7 = (8.8 \pm 0.5) \times 10^6\ M^{-1}\ s^{-1}$ [a]	
8	$Cl_2^{-\bullet} + S_2O_8^{2-} \rightarrow$ products	$k_8 \leq 1 \times 10^4\ M^{-1}\ s^{-1}$ [a]	
9	$Cl_2^{-\bullet} + Cl_2^{-\bullet} \rightarrow Cl_2 + 2Cl^-$	$k_9 = (9 \pm 1) \times 10^8\ M^{-1}\ s^{-1}$ [a,9]	
10	$Cl_2^{-\bullet} + Cl \rightarrow Cl_2 + Cl^-$	$k_{10} = (2.1 \pm 0.05) \times 10^9\ M^{-1}\ s^{-1}$ [a]	
11	$SO_4^{-\bullet} + SO_4^{-\bullet} \rightarrow S_2O_8^{2-}$	$k_{11} = (6.1 \pm 0.15) \times 10^8\ M^{-1}\ s^{-1}$ [a]	
12	$SO_4^{-\bullet} + S_2O_8^{2-} \leftrightarrow SO_4^{2-} + S_2O_8^{-\bullet}$	$k_{12} = (5.5 \pm 0.3) \times 10^5\ M^{-1}\ s^{-1}$ [a]	
13	$SO_4^{-\bullet} + H_2O \rightarrow HSO_4^- + HO^\bullet$	$k_{13}[H_2O] = 460 \pm 90\ s^{-1}$ [a]	$k_{-13} = 6.9 \times 10^5\ M^{-1}\ s^{-1}$ [46]
14	$HSO_4^- \leftrightarrow SO_4^{2-} + H^+$	$K_{14} = 1.2 \times 10^{-2}\ M^{-1}$ [117]	

[a] This work, errors are within $\pm 1\sigma$.

Pulse radiolysis and flash photolysis techniques have been used to study systems containing chloride ions and sulfate radicals.[14−24] In our laboratory, sulfate radicals are generated by laser flash photolysis of persulfate ions in aqueous solutions via reaction 1 (see Table 1; in this paper, rate constants, k_i, are written in lower case, while equilibrium constants, K_i, are written in upper case).

There has been considerable previous research investigating the kinetics, as well as determining the absorption spectra, of $Cl_2^{-\bullet}$ and $SO_4^{-\bullet}$.[15,16,18−20,24,29,34−72] Discrepancies in the peak molar extinction coefficients of $Cl_2^{-\bullet}$ and $SO_4^{-\bullet}$ still exist, however. Because of overlap between the spectra of $Cl_2^{-\bullet}$ and $SO_4^{-\bullet}$ and because the spectra are broad and featureless, spectral interference is always present. Thus, careful determinations of the absorption spectra for the two species are reported here.

Similar to the reactions of $Cl^\bullet$ and $Cl_2^{-\bullet}$ with H_2O_2,[9] $Cl^\bullet$ and $Cl_2^{-\bullet}$ may react with $S_2O_8^{2-}$ according to reactions 7 and 8 (also see Buxton et al.[24]). The participation of reactions 3−5 in the decay of $Cl_2^{-\bullet}$ leads to the prediction of a pH dependence, which has not been observed unambiguously in previous experimental work. We report the first experimental observation of the predicted pH dependence. Most previous studies of the second-order decay of $Cl_2^{-\bullet}$ [9,18−20,23,73] were carried out under conditions of high Cl^- molar concentration, where reaction 9 is dominant. At low Cl^- molar concentration ($<1 \times 10^{-3}$ M), we have found that reaction 10 also contributes to the second-order loss of $Cl_2^{-\bullet}$. This is not surprising, since $Cl^\bullet$ and $Cl_2^{-\bullet}$ form an equilibrium with $Cl_3^{-\bullet}$,[74] which can subsequently dissociate into Cl_2 and Cl^-.[54,75−77]

Since $Cl_2^{-\bullet}$ and $SO_4^{-\bullet}$ were monitored simultaneously in this work, the rise and decay of $SO_4^{-\bullet}$ was also investigated. Our results for the pseudo-first-order rate constant and second-order rate constant of $SO_4^{-\bullet}$ decay are found to be consistent with literature values.

In the following sections, we first present the chemical mechanism and a discussion of the relevant literature. Afterward, we briefly describe our experimental techniques and the determination of the absorption spectra of $Cl_2^{-\bullet}$ and $SO_4^{-\bullet}$. We then go on to explain how we tested the accuracy of the mechanism and carried out measurements of rate constants. Finally, we present the results and discuss them in relation to the literature.

2. Chemical Mechanism (Table 1)

2.1. Kinetics of $Cl_2^{-\bullet}$. The photodissociation of persulfate ions generates sulfate radicals ($SO_4^{-\bullet}$) via reaction 1. Under neutral and alkaline conditions, $Cl_2^{-\bullet}$ is produced efficiently by reaction 2, followed by reaction 3.[14−24] Rate constant k_{-2} and equilibrium constant K_2 have been reported.[21,24] The loss of Cl_2^- follows a mixed first- and second-order mechanism.[9,19,60,78−81] Reactions 4 and 6 are for $Cl^{\bullet}$ and $Cl_2^{-\bullet}$ with H_2O; analogous reactions occur for $Cl^{\bullet}$ and $Cl_2^{-\bullet}$ with H_2O_2.[9] We propose the similar reactions 7 and 8 for $Cl^{\bullet}$ and $Cl_2^{-\bullet}$ with $S_2O_8^{2-}$.

Reaction −4 introduces a pH dependence into the mechanism. Our present experiments on the pseudo-first-order decay of $Cl_2^{-\bullet}$ show a dependence on H^+ molar concentration, in contrast to earlier experimental results[19,44,82] yet supporting their theoretical predictions.

Under relatively high Cl^- molar concentration, the second-order decay of $Cl_2^{-\bullet}$ takes place mainly via reaction 9.[9,18−20,23,73] At $[Cl^-] < 1 \times 10^{-3}$ M, the present work (see below) shows that reaction 10 contributes to the second-order loss of $Cl_2^{-\bullet}$ to produce Cl_2 and Cl^- [54,75−77] via the equilibrium of $Cl^{\bullet}$ and $Cl_2^{-\bullet}$ with $Cl_3^{-\bullet}$.[74]

2.2. Kinetics of $SO_4^{-\bullet}$. The decay of $SO_4^{-\bullet}$ follows mixed first- and second-order kinetics.[18,19,24,29,34−44] Sulfate radicals reacting with Cl^-, $S_2O_8^{2-}$, and H_2O (reactions 2, 12, and 13) produce the pseudo-first-order contribution to the decay; reaction 11 makes the second-order contribution. Equilibrium 14 is included in the mechanism for completeness.

3. Experimental Section

3.1. Apparatus. The experimental apparatus is similar to that used in other work from this laboratory.[9,10,12,13,23,41,83] Briefly, a pulsed rare gas−halogen excimer laser was used to photolyze solutions containing persulfate ions and chloride ions at 248 nm. The laser pulse energy was monitored by a diode detector behind the reaction cell for all experiments run and calibrated daily. The detailed experimental approach is published elsewhere.[10] A high-pressure xenon−mercury arc lamp provided a continuous light source for monitoring transient species by absorption. Dichloride radical anion ($Cl_2^{-\bullet}$) was monitored by its absorption at 364 nm, the wavelength of the strongest output band of the xenon−mercury lamp in the vicinity of the $Cl_2^{-\bullet}$ absorption maximum (∼340 nm). The absorption coefficient of the radicals is found in the present work (see below) to be $\epsilon(Cl_2^{-\bullet},364\text{ nm}) = 7000 \pm 700\ M^{-1}\ cm^{-1}$ (base 10). Under the experimental conditions used in this work, the concentration of solvated $Cl^{\bullet}$ atoms is very low, and their light absorption (absorption coefficient[84,85] $\epsilon(Cl^{\bullet},364\text{ nm}) \approx 2000\ M^{-1}\ cm^{-1}$ (base 10)) can be neglected compared to that of $Cl_2^{-\bullet}$ (see below). White cell optics were utilized to fold the optical path in the cell to enhance detection sensitivity.[86] A monochromator equipped with a photomultiplier was used to monitor the transmitted light. The photomultiplier tube output was amplified and sent to a digital oscilloscope for signal averaging and thence to a computer for data analysis. Least-squares fits of the experimental data were carried out using KaleidaGraph[87] software, which utilizes the Levenberg−Marquardt nonlinear least-squares algorithm.[88] The fitting uncertainty is always within 5% with R^2 better than 0.98. The uncertainties for the recommended values from this work correspond to $\pm\sigma$, obtained from propagation of errors.

3.2. Reagents. All solutions were prepared immediately before the experiments. The water was purified by a Milli-RO/Milli-Q system (the water resistivity was ≥18 MΩ cm). All reagents were of ACS grade. Sodium chloride (99.999%) and anhydrous sodium perchlorate (98−102%) were purchased from Alfa ÆSR and used without further purification. Perchloric acid ($HClO_4$, 70%) was purchased from Aldrich. Potassium persulfate ($K_2S_2O_8$ ≥ 99.0%) was obtained from Fisher Scientific. The concentration of $K_2S_2O_8$ utilized in the experiments was usually $\sim 10^{-3}$ M. The pH (0−4) of all solutions was controlled by adding perchloric acid ($HClO_4$) and measured with a Digital Ionalyzer (Orion Research 501) calibrated with appropriate pH buffer solutions (Fisher).

All experiments were carried out at room temperature (297 ± 2 K), except in the study of the k_9 temperature dependence, where the solution temperature was controlled in the range of 6.8−51.6 °C by a constant-temperature water bath. The solutions contained dissolved air, unless specifically mentioned otherwise. In some experiments, the dissolved air was purged by bubbling with argon gas (99.999%, Liquid Carbonic Corporation). Dissolved air was found to have no detectable effect on the kinetics of the system.

4. Results

4.1. Absorption Spectra of $Cl_2^{-\bullet}$ and $SO_4^{-\bullet}$. Interference between $Cl_2^{-\bullet}$ and $SO_4^{-\bullet}$ absorption has often been circumvented by detecting $SO_4^{-\bullet}$ at a wavelength between 440 and 510 nm, where the $Cl_2^{-\bullet}$ absorption is small,[15,18,20,21,23] while probing $Cl_2^{-\bullet}$ around the peak of its absorption near 340 nm,[16,20−22,24,89] where the $SO_4^{-\bullet}$ absorption is small. To ensure the quality of our kinetics results, we measured the absorption spectra of both species. In analyzing the results to obtain quantitative absorption coefficients, we assume that the quantum yield of sulfate radical formation in reaction 1 is $\Phi_{SO_4^{-\bullet}} = 2$, in agreement with previous work.[29,32,37,50] This assumption is further supported by the virtually exact agreement of the results obtained below with other recent determinations of $\epsilon_{SO_4^{-\bullet}}$[53] and $\epsilon_{Cl_2^{-\bullet}}$.[65,71]

4.1.1. The Absorption Spectrum of $SO_4^{-\bullet}$. The absorption spectrum of sulfate radicals was determined at 5 nm intervals between 300 and 550 nm by laser flash photolysis of persulfate ions at 248 nm. The relative absorption spectrum of $SO_4^{-\bullet}$ has been determined previously in our laboratory by laser flash photolysis of $S_2O_8^{2-}$ in a wide range of acidic conditions, that is, $0 \le [H^+] \le 2.0$ M.[37,41] It was concluded that $SO_4^{-\bullet}$ radical and its protonated form HSO_4^- have the same spectrum.

The molar extinction coefficient of sulfate radical, $\epsilon_{SO_4^{-\bullet}}$, is expressed in eq Ia

$$\epsilon_{SO_4^{-\bullet}} = \frac{A_0(SO_4^{-\bullet})}{s\Phi_{SO_4^{-\bullet}}\alpha_{S_2O_8^{2-}}[S_2O_8^{2-}]_0 F_\lambda} \qquad \text{(Ia)}$$

where $A_0(SO_4^{-\bullet})$ is the initial absorbance of $SO_4^{-\bullet}$; s is the path length; $\Phi_{SO_4^{-\bullet}}$ is the quantum yield of $SO_4^{-\bullet}$ in the photodissociation of $S_2O_8^{2-}$; $\alpha_{S_2O_8^{2-}}$ is the molar extinction coefficient of $S_2O_8^{2-}$ at the photolysis wavelength; $[S_2O_8^{2-}]$ is the concentration of $S_2O_8^{2-}$; and F_λ is the photolysis laser fluence.

The molar extinction coefficient of persulfate ions at 248 nm is $\alpha_{S_2O_8^{2-}} = 25\ M^{-1}\ cm^{-1}$ (base 10).[15,27,37,39,90] With the assumption that $\Phi_{SO_4^{-\bullet}} = 2$,[29,32,37,50] an upper limit to $\epsilon_{SO_4^-}$ can be obtained from measurements of the laser power, the absorbance, and the other parameters in eq Ia. The spectrum of $SO_4^{-\bullet}$ determined in this manner is shown in Figure 2.

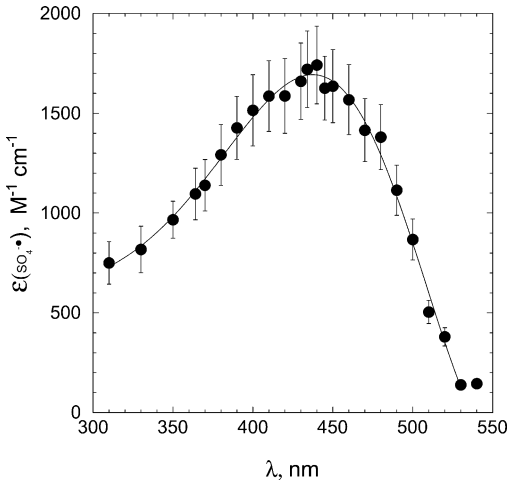

Figure 2. The absorption spectrum of $SO_4^{-\bullet}$. The error bars (propagated, $\pm 1\sigma$) correspond to precision only.

TABLE 2: Comparison of the Molar Extinction Coefficient of $SO_4^{-\bullet}$ at 450 nm

$\epsilon_{SO_4^{-\bullet}}$, M^{-1} cm^{-1} (base 10)	$\epsilon_{SO_4^{-\bullet}} \cdot \Phi_{SO_4^{-\bullet}}$ (base 10)	method[a]	reference
1050		PR	1966[46]
1100[b]		PR	1969[47]
1100		PR	1972[36]
1600		PR	1975[15]
1600 ± 100		PR	1990[39]
1570 ± 130		PR	1992[40]
1630 ± 120		PR	1992[40]
1700 ± 150		PR	1992[40]
1630 ± 50		PR	1996[53]
450 ± 45		FP	1967[34]
460 ± 25		FP	1967[29,35]
1385 ± 140[c]	2770 ± 280	FP	1988[37]
1385 ± 275[c]	2770 ± 550	FP	1988[50]
1300 ± 300[d]		FP	1989[18]
1630 ± 10[e]	3260 ± 20	FP	this work, 2003

[a] PR, pulse radiolysis; FP, flash photolysis. [b] Observed at 460 nm. [c] Measured at 443 nm and derived with $\Phi_{SO_4^{-\bullet}} = 2$ assumption. [d] The conclusion is based upon ~445 nm. [e] The error was from fitting uncertainty with error propagation $\epsilon_{SO_4^{-\bullet},450\ nm} = 1630 \pm 180\ M^{-1}\ cm^{-1}$ (base 10).

The values for $\epsilon_{SO_4^{-\bullet}}$ at the absorption maximum (450 nm) from the literature and from the present work are listed in Table 2. Our result of $\epsilon_{SO_4^{-\bullet}} = 1630 \pm 180\ M^{-1}\ cm^{-1}$ (base 10) is in fair agreement with a previous laser flash photolysis measurement[50] of $\epsilon_{SO_4^{-\bullet}} = 1385\ M^{-1}\ cm^{-1}$ (assuming $\Phi_{SO_4^{-\bullet}} = 2$). However, it is in excellent agreement with recent pulse radiolysis measurements (see Table 2 where the assumption of $\Phi_{SO_4^{-\bullet}} = 2$ is not necessary), giving additional support to the conclusion that $\Phi_{SO_4^{-\bullet}} = 2$.

4.1.2. The Absorption Spectrum of $Cl_2^{-\bullet}$. A scavenger method was used to determine $\epsilon_{Cl_2^{-\bullet}}$ using the mechanism in Table 1. With optimum scavenging, $[SO_4^{-\bullet}]_0 = [Cl_2^{-\bullet}]_0$ and the expression of $\epsilon_{Cl_2^{-\bullet}}$ is given by eq Ib.

$$\epsilon_{Cl_2^{-\bullet}} = \frac{A_0(Cl_2^{-\bullet})}{s\Phi_{SO_4^{-\bullet}}\alpha_{S_2O_8^{2-}}[S_2O_8^{2-}]_0 F_\lambda} \qquad \text{(Ib)}$$

Once again, $\Phi_{SO_4^{-\bullet}} = 2$ is assumed.

The dichloride anion radical, $Cl_2^{-\bullet}$, was produced by laser flash photolysis of solutions containing 0.1 M NaCl and 3×10^{-3} M $K_2S_2O_8$. The spectrum of $Cl_2^{-\bullet}$ at the interval of 5 nm from 230 to 450 nm determined in this work is shown in Figure 3. The peak of the $Cl_2^{-\bullet}$ absorption is found at 340 nm, where the molar extinction coefficient is $8500 \pm 500\ M^{-1}\ cm^{-1}$ (base 10). Values for $\epsilon_{Cl_2^{-\bullet}}$ at 340 nm are summarized in Table 3. Our result is in excellent agreement with results from both pulse radiolysis and flash photolysis,[54−64,40,65−72,91] which supports the assumption that $\Phi_{SO_4^{-\bullet}}$ is 2.

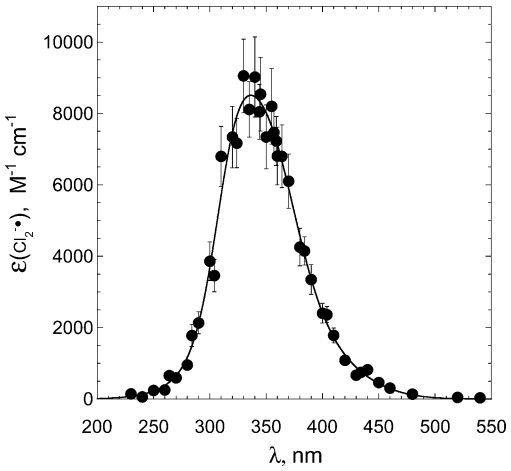

Figure 3. The absorption spectrum of $Cl_2^{-\bullet}$. The error bars (propagated, $\pm 1\sigma$) correspond to precision only.

TABLE 3: Comparison of the Molar Extinction Coefficient of $Cl_2^{-\bullet}$ at 340 nm

$\epsilon_{Cl_2^{-\bullet}}$, M^{-1} cm^{-1} (base 10)	method[a]	reference
12500 ± 1000	PR	1964,[57] 1976[103]
8800 ± 500	PR	1973[60]
9580 ± 100	PR	1973[75]
8700	PR	1975[62]
8600[b]	PR	1976[89]
8100	PR	1977,[118] 1980,[105] 1987[66,119]
12001[c]	PR	1989[67]
9600	PR	1995[71]
8800 ± 650	PR	2003[91]
9000	FP	1972,[120,121] 1985[65]
8500 ± 500[d]	FP	this work, 2003

[a] PR, pulse radiolysis; FP, flash photolysis. [b] This measurement is done at 345 nm. [c] The maximum is assigned at 350 nm. [d] The uncertainty is propagated error with $\pm 1\sigma$.

In our previous determination of quantum yield of the hydroxyl radicals in the photolysis of aqueous hydrogen peroxide,[10] the absorption coefficient $\epsilon_{Cl_2^{-\bullet}}$ for $Cl_2^{-\bullet}$ radicals was required. The accuracy of $\epsilon_{Cl_2^{-\bullet}}$ depends on the validity of the assumption of $\Phi_{SO_4^{-\bullet}} = 2$. Ultimately, the quantum yield of hydroxyl radicals derived in that work is relative to that of sulfate radicals.[92]

4.2. Absorbance Analysis. Since the spectra of $Cl_2^{-\bullet}$ and of $SO_4^{-\bullet}$ overlap, caution is needed in analyzing the absorbance data used to determine the reaction kinetics. In this work, $SO_4^{-\bullet}$ was monitored at 450 nm ($\epsilon(SO_4^{-\bullet},450\ nm) = 1630\ M^{-1}\ cm^{-1}$ (base 10), this work), where the monitoring lamp has high intensity and the $Cl_2^{-\bullet}$ absorption is much weaker than that of $SO_4^{-\bullet}$. Similarly, $Cl_2^{-\bullet}$ was monitored at 364 nm, where the radical anion has sufficiently strong absorption ($\epsilon(Cl_2^{-\bullet},364\ nm) = 7000\ M^{-1}\ cm^{-1}$ (base 10), this work) and the monitoring lamp is relatively bright.

The observed absorption is the sum of $A(Cl_2^{-\bullet})_t$ and $A(SO_4^{-\bullet})_t$, A_{total}, expressed in eqs IIa and IIb corresponding to the sum of eqs III ($A(Cl_2^{-\bullet})_t$) and X ($A(SO_4^{-\bullet})_t$). The detailed derivation of $A(Cl_2^{-\bullet})_t$ is presented in Paper I,[9] and $A(SO_4^{-\bullet})_t$ is readily

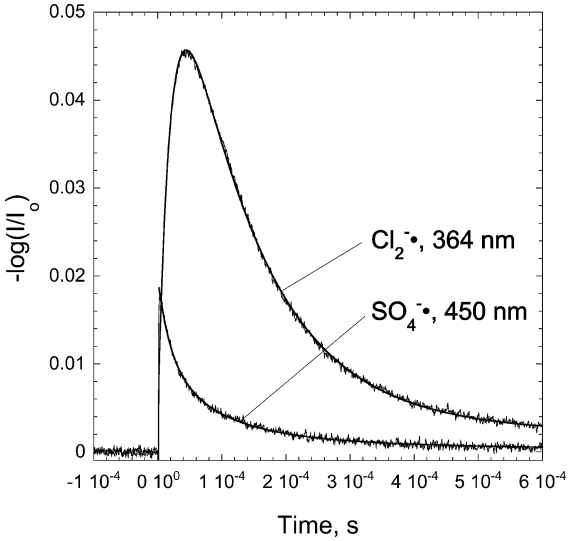

Figure 4. Typical time profiles of $Cl_2^{-\bullet}$ and $SO_4^{-\bullet}$ monitored at 364 and 450 nm, respectively, at $[S_2O_8^{2-}] = 3 \times 10^{-3}$ M, $[Cl^-] = 5 \times 10^{-5}$ M, and pH = 0. The solid lines are nonlinear least-squares fits.

obtained by using the expression for mixed first- and second-order kinetics:

$$A_{\text{total}} = \epsilon_{Cl_2^{-\bullet}} s C[e^{-k_A t} - e^{-k_B t}] + \left\{ \exp(k^{I}_{SO_4^{-\bullet}} t)\left(\frac{1}{A(SO_4^{-\bullet})_0} + \frac{2k_{SO_4^{-\bullet}}}{\epsilon_{SO_4^{-\bullet}} s k^{I}_{SO_4^{-\bullet}}}\right) - \frac{2k_{SO_4^{-\bullet}}}{\epsilon_{SO_4^{-\bullet}} s k^{I}_{SO_4^{-\bullet}}} \right\}^{-1} \quad \text{(IIa)}$$

where s is the optical path length, C is a constant (see Paper I[9]), k_A is the observed pseudo-first-order rate constant corresponding to the rise of $Cl_2^{-\bullet}$, k_B is the observed pseudo-first-order rate constant corresponding to the decay of $Cl_2^{-\bullet}$, $k^{I}_{SO_4^{-\bullet}}$ is the pseudo-first-order rate constant of $SO_4^{-\bullet}$ decay, and $k_{SO_4^{-\bullet}}$ is the observed second-order rate constant of $SO_4^{-\bullet}$ decay.

When $SO_4^{-\bullet}$ molar concentration is low, the principal decay routes of $SO_4^{-\bullet}$ are pseudo-first-order via reactions 2, 12, and 13. The total absorption, A_{total}, given by eq IIa reduces to eq IIb:

$$A_{\text{total}} = \epsilon_{Cl_2^{-\bullet}} s C[e^{-k_A t} - e^{-k_B t}] + A(SO_4^{-\bullet})_0 \exp(-k^{I}_{SO_4^{-\bullet}} t) \quad \text{(IIb)}$$

Typical time profiles of $Cl_2^{-\bullet}$ and $SO_4^{-\bullet}$ monitored simultaneously at 364 and 450 nm, respectively, are shown in Figure 4. The solid lines are nonlinear least-squares fits using eq IIb. The analysis of $Cl_2^{-\bullet}$ and $SO_4^{-\bullet}$ data is explained in more detail in the following sections.

4.3. Kinetics Analysis. The present system, involving $SO_4^{-\bullet}$ and Cl^-, is similar in some ways to the system containing $HO^\bullet$ and Cl^-.[9] This is especially true of the rise and decay of $Cl_2^{-\bullet}$ under conditions of low Cl^- molar concentration. The decay of $Cl_2^{-\bullet}$ is an important focus in this work. In the present work, $SO_4^{-\bullet}$ and $Cl_2^{-\bullet}$ time profiles are monitored simultaneously, and then the rise and decay of each radical is analyzed. We report the analysis of $Cl_2^{-\bullet}$ first and then that of $SO_4^{-\bullet}$.

4.3.1. Strategy. The mechanism shown in Table 1 and Figure 1 is complicated but can be simplified considerably under controlled experimental conditions. The $Cl_2^{-\bullet}$ formation takes place via reactions 1−3 as concluded by earlier research,[14−24,43,81,89,93−95] and its loss takes place via reactions 4−10, hence, following mixed first- and second-order kinetics.[9,19,60,78,79,81,96]

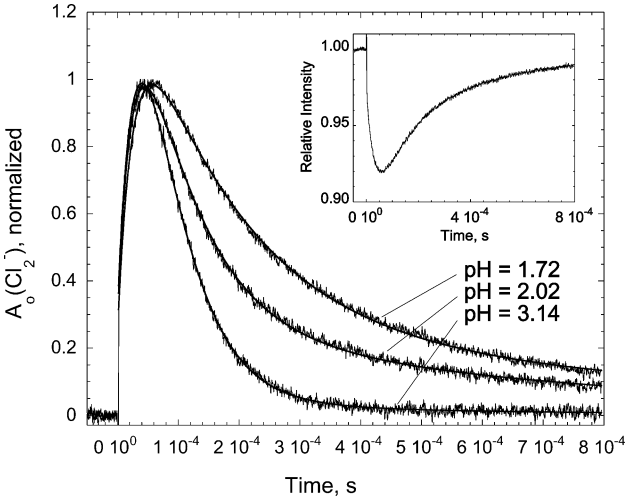

Figure 5. Some typical time profiles of $Cl_2^{-\bullet}$ under various pH conditions. The solid lines are nonlinear least-squares fits. The experimental conditions are $[NaCl] = 4 \times 10^{-4}$ M, $[K_2S_2O_8] = 2 \times 10^{-3}$ M, and pH = 1.72, 2.02, and 3.14 all controlled by adding $HClO_4$. The insert is a time profile of $Cl_2^{-\bullet}$ observed at higher $[Cl^-]$ fit with mixed first- and second-order kinetics for its decay.

For $[Cl^-] < 1 \times 10^{-3}$ M, the observed loss of $Cl_2^{-\bullet}$ is mainly first-order because the second-order contribution is insignificant due to low $Cl_2^{-\bullet}$ molar concentration. Therefore, analyses of the experimental data obtained for $[NaCl] < 1 \times 10^{-3}$ M were analyzed by solving the mechanism as pseudo-first-order consecutive reactions.[9,97] The mixed first- and second-order scheme was also used for comparison. From the mixed first- and second-order analysis, it was found that the second-order contribution is essentially negligible. Hence, the second-order reactions are neglected in most of the following analysis of the rise and decay of $Cl_2^{-\bullet}$ under low Cl^- molar concentration, similar to the strategy adopted in Paper I.[9]

At lower Cl^- molar concentration, reaction 10 contributes to the second-order loss of $Cl_2^{-\bullet}$ in addition to reaction 9. Therefore, the most important reactions related to $Cl_2^{-\bullet}$ in Table 1 are reactions ±2, ±3, ±4, and 6−10. In the following analysis, we obtain values for rate constants, equilibrium constants, or both for most of these reactions under conditions that minimize interferences and correlations in the least-squares analysis. We do not apply any estimated adjustments for ionic strength in the following analysis because the ionic strength is nearly constant (∼0.01 M) in all of the experiments. Moreover, the estimated effects are relatively small (∼20%), as described in section 5.1 where we specifically investigate the effect of ionic strength on k_2 and k_9.

Typical time profiles (normalized for ease of comparison) of the rise and decay of $Cl_2^{-\bullet}$ under various pH conditions at constant NaCl molar concentration ($\leq 10^{-3}$ M) and $S_2O_8^{2-}$ molar concentration are shown in Figure 5. The solid lines are nonlinear least-squares fits to eq III. The rise time of $Cl_2^{-\bullet}$ molar concentration corresponds to the faster step of $Cl_2^{-\bullet}$ production and loss, whereas the fall time corresponds to the slower step.[9,97,98] The rise time of the $Cl_2^{-\bullet}$ absorption signals is very rapid, regardless of pH. In contrast, the rate of the signal decay decreases as H^+ molar concentration increases. Since the formation of $Cl_2^{-\bullet}$ does not involve H^+, the signal decay time corresponds to the loss of $Cl_2^{-\bullet}$. This pH dependence of the $Cl_2^{-\bullet}$ decay is examined in detail below. First, we investigate the $Cl_2^{-\bullet}$ rise and decay at constant pH.

The analytical solution for $Cl_2^{-\bullet}$ molar concentration at constant pH is expressed by eq III, which is derived in a manner

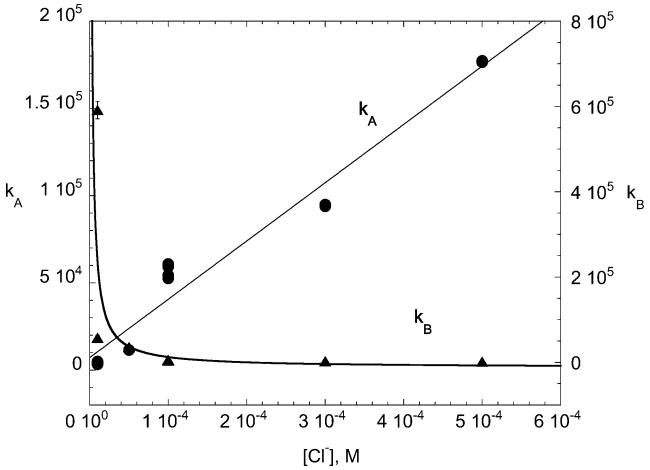

Figure 6. Plots of k_A and k_B vs $[Cl^-]$. The solid lines are least-squares fits. The circle is k_A, and the triangle is k_B (unit, s^{-1}). The error bars ($\pm 1\sigma$) are usually approximately the size of or smaller than the markers.

exactly analogous to the derivation presented in the Appendix of Paper I.[9]

$$A(Cl_2^{-\bullet})_t = \epsilon_{Cl_2^-} sC[e^{-k_A t} - e^{-k_B t}] \qquad \text{(III)}$$

The expressions for k_A and k_B are given by eqs IV and V, respectively:

$$k_A = k_{12}[S_2O_8^{2-}] + k_2[Cl^-] \qquad \text{(IV)}$$

$$k_B = \frac{k_3[Cl^-]\beta + \alpha(k_{-3} + \beta)}{k_3[Cl^-] + k_{-3} + \alpha + \beta} \qquad \text{(V)}$$

where $\alpha = k_7[S_2O_8^{2-}] + k_{-4}[H_2O]$ and $\beta = k_8[S_2O_8^{2-}] + k_6[H_2O]$. When equilibrium 3 is maintained, that is, when $K_3 = k_3/k_{-3}$, and $k_3[Cl^-] + k_{-3} \gg \alpha + \beta$, k_B reduces to eqs VIa and VIb:

$$k_B = \frac{k_6K_3[Cl^-] + k_4}{K_3[Cl^-] + 1}[H_2O] + \frac{k_8K_3[Cl^-] + k_7}{K_3[Cl^-] + 1}[S_2O_8^{2-}] \qquad \text{(VIa)}$$

or

$$k_B = I + S[S_2O_8^{2-}] \qquad \text{(VIb)}$$

Equation VI is very useful in the analysis of the experimental data.

Rate constants k_A and k_B, which are functions of both $S_2O_8^{2-}$ and Cl^- molar concentrations, can be determined from data such as those shown in Figure 6. From the least-squares fit of a single experiment, it is only possible to find two fitted rate constants, and it is not possible to identify which rate constant corresponds to k_A and which k_B. However, by carrying out experiments over a range of Cl^- molar concentration (refer to eqs IV and V), one can identify the rate constants: the one linearly proportional to Cl^- molar concentration is identified as k_A (in eq IV), and the other is identified as k_B (in eq V). This identification is unambiguous, as is apparent from the representative data shown in Figure 6.

4.3.2. Analysis Based on k_A. Fitted rate constant k_A in eq IV depends on rate constants k_2 and k_{12}. The directly measured and derived results for k_2 and k_{12} are summarized in Table 4. A plot of k_A vs $[Cl^-]$ at pH 2 is shown in Figure 6. Rate constant

TABLE 4: Summary of Results from k_A Analysis at Room Temperature

method	source	directly measured results
k_A−$[Cl^-]$ linear fit	slope	$k_2 = (3.3 \pm 0.2) \times 10^8\ M^{-1}\ s^{-1}$
	intercept	$k_{12} < 2.0 \times 10^6\ M^{-1}\ s^{-1}$

$k_2 = (3.3 \pm 0.2) \times 10^8\ M^{-1}\ s^{-1}$ is obtained from the slope of the linear least-squares fit; the intercept depends on k_{12}.

4.3.3. Analysis Based on k_B. First-Order Reaction. The loss of $Cl_2^{-\bullet}$ is assumed to follow mixed first- and second-order kinetics.[9,19,60,78,79,81,96] A typical time profile of $Cl_2^{-\bullet}$ produced by laser flash photolysis of Cl^- and $S_2O_8^{2-}$ at constant pH and detected at 364 nm is shown in the insert panel of Figure 5. Reactions 4, 6, 7, and 8 contribute to the first-order loss of $Cl_2^{-\bullet}$. The study of $Cl_2^{-\bullet}$ loss as a function of $S_2O_8^{2-}$ and Cl^- molar concentrations was studied at constant pH to avoid the predicted pH dependence. The predicted pH dependence of $Cl_2^{-\bullet}$ loss was investigated at constant $S_2O_8^{2-}$ and Cl^- molar concentrations.

Dependence on $S_2O_8^{2-}$ and Cl^- Molar Concentrations. Reactions 4 and 6 are thought to be the main routes for the pseudo-first-order loss of $Cl_2^{-\bullet}$. In controlled experiments, it was found that as NaCl molar concentration increases, k_B decreases, as observed previously.[19,23,81] In experiments in which $S_2O_8^{2-}$ molar concentration was varied, the NaCl molar concentration was kept constant to exclude the effects of reactions 4 and 6. However, k_B was found to change systematically as $S_2O_8^{2-}$ molar concentration varied. The major impurity in all available sources of $K_2S_2O_8$ is sulfuric acid, which tends to control the pH of $K_2S_2O_8$ solutions. For example, McElroy[19] reported that a 0.4 M solution of $K_2S_2O_8$ had a pH of ~4, equivalent to a H_2SO_4 content of ~0.2%. We find a similar effect in our experiments.[18,81] To eliminate the pH effect caused by the impurity, the pH of all solutions was controlled by adding $HClO_4$. The pH in the experiments discussed here was fixed at 2, which is much lower than the unadjusted pH.[19,99]

Under conditions where both pH and NaCl molar concentration are held constant, k_B was observed to increase as $K_2S_2O_8$ molar concentration increased, which indicates that $Cl_2^{-\bullet}$ or Cl reacts with $S_2O_8^{2-}$ on the experimental time scale. When equilibrium 3 is maintained with $[S_2O_8^{2-}] \leq 1$ mM, the fitted rate constant k_B varies linearly with $S_2O_8^{2-}$ molar concentration as shown in Figure 7. The solid lines are linear least-squares fits to eq VI. When $K_3[Cl^-] \gg 1$ is satisfied, the slope (S) and intercept (I) of each line in Figure 7 depend on Cl^- molar concentration as follows:

$$I = \frac{k_4[H_2O]}{K_3[Cl^-]} + k_6[H_2O] = \frac{S_I}{[Cl^-]} + I_I \qquad \text{(VIIa)}$$

$$S = \frac{k_7}{K_3[Cl^-]} + k_8 = \frac{S_s}{[Cl^-]} + I_s \qquad \text{(VIIb)}$$

where $S_I = k_4[H_2O]/K_3$, $I_I = k_6[H_2O]$, $S_s = k_7/K_3$, and $I_S = k_8$. The slopes and intercepts are plotted vs 1/[NaCl] in Figure 8a,b, and a linear least-squares analysis gives values for k_7/K_3, k_8, $k_4[H_2O]/K_3$, and $k_6[H_2O]$ summarized in Table 5.

Dependence on pH. At low Cl^- molar concentration, the contribution of $Cl^\bullet$ atom reactions to the overall loss of $Cl_2^{-\bullet}$ becomes more important, due to reactions 4 and 7. When $S_2O_8^{2-}$ molar concentration is held fixed, the variation of k_B should be caused solely by reactions 4 and −4, which are assumed to be at equilibrium. As H^+ molar concentration increases, the overall first-order reaction rate of $Cl_2^{-\bullet}$ loss becomes slower because the rate of reaction −4 becomes larger. It is observed here that

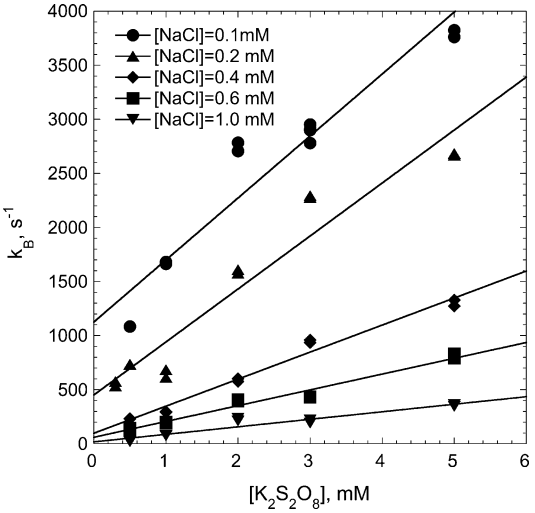

Figure 7. The k_B dependence on $[S_2O_8^{2-}]$ and $[Cl^-]$. The solid lines are linear least-squares fits to eq VI. The pH of all experiments shown was 2 controlled by adding $HClO_4$. The circle is 0.1 mM NaCl, triangle 0.2 mM NaCl, diamond 0.4 mM NaCl, square 0.6 mM NaCl, and inverse triangle 1.0 mM NaCl. The error bars ($\pm 1\sigma$) are usually approximately the size of or smaller than the markers.

k_B depends on pH when $S_2O_8^{2-}$ and Cl^- molar concentrations are held constant, as shown in Figure 5. When equilibria 2 and 3 are maintained, k_B can be expressed by eq VIII (derived in Appendix A):

$$k_B = \frac{1}{K_3[Cl^-]} \times \left\{ k_4[H_2O] + k_7[S_2O_8^{2-}] - \frac{k_4[H_2O]}{1 + k_x/(k_{-4}[H^+])} \right\} \quad \text{(VIII)}$$

where $k_x = k_{5a}[Cl^-] + k_{5b}[Cl] + k_{5c}[SO_4^{-\bullet}] + k_{5d}[S_2O_8^{2-}] + k_{5'}$. The dependence of k_B on H^+ molar concentration at constant $[S_2O_8^{2-}] = 2$ mM and Cl^- molar concentration is shown in Figure 9.

The solid lines in Figure 9 are nonlinear least-squares fits using eq VIII. Three fitting parameters are obtained directly from the nonlinear least-squares fits of k_B vs H^+ molar concentration: $c_1 = k_4[H_2O]/(K_3[Cl^-])$, $c_2 = k_7[S_2O_8^{2-}]/(K_3[Cl^-])$, and $c_3 = k_x/k_{-4}$ (Table 6). The first two parameters are simply linearly dependent on the inverse of Cl^- molar concentration. By plotting the fitted values of c_1 and c_2 with respect to $1/[Cl^-]$ and using linear least-squares fits to analyze the result, we obtain $k_4[H_2O]/K_3 = 1.1 \pm 0.1$ M s^{-1} and $k_7[S_2O_8^{2-}]/K_3 = 0.12 \pm 0.01$ M s^{-1}. These two parameters were also obtained in the analysis of k_B dependence on $S_2O_8^{2-}$ and Cl^- molar concentrations at a constant pH as listed in Table 5.

The analysis of $c_3 = k_x/k_{-4}$ is more complicated, because it is associated with the loss of $ClOH^{-\bullet}$ via the following reactions:

$$ClOH^{-\bullet} \rightarrow OH^- + Cl^{\bullet} \quad (5')$$

$$ClOH^{-\bullet} + Cl^- \rightarrow OH^- + Cl_2^{-\bullet} \quad (5a)$$

$$ClOH^{-\bullet} + Cl^{\bullet} \rightarrow HO^{\bullet} + Cl_2^{-\bullet} \quad (5b)$$

$$ClOH^{-\bullet} + SO_4^{-\bullet} \rightarrow Cl^- + HSO_5^- \quad (5c)$$

$$ClOH^{-\bullet} + S_2O_8^{2-} \rightarrow Cl^{\bullet} + HSO_5^- + SO_4^{-\bullet} \quad (5d)$$

Because Cl^- molar concentration is much larger than $ClOH^{-\bullet}$ molar concentration in this system, the reverse reaction -5 counteracts the forward reaction 5, making it an inefficient path for $ClOH^{-\bullet}$ decay.

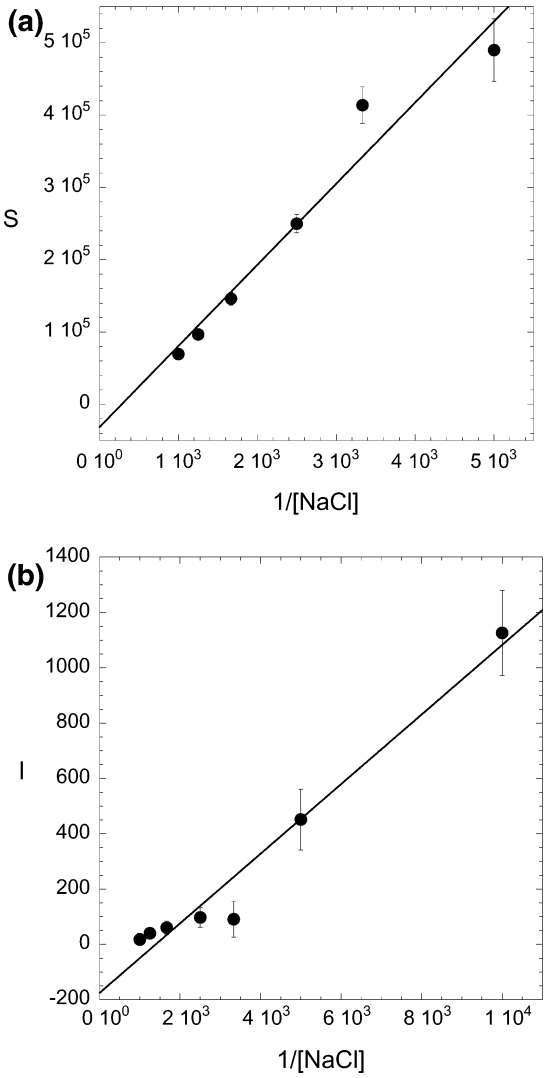

Figure 8. The plots of (a) S and (b) I vs 1/[NaCl]. The solid line is linear least-squares fit. The error bars ($\pm 1\sigma$) are usually approximately the size of or smaller than the markers.

TABLE 5: Summary of Directly Measured and Derived Results from k_B Dependence on $S_2O_8^{2-}$ and Cl^- Molar Concentrations at pH 2

directly measured results	derived results
$k_4[H_2O]/K_3 = 1.2 \pm 0.1$ M s^{-1}	$k_4[H_2O] = (1.7 \pm 0.1) \times 10^5$ s^{-1}
$k_6[H_2O] \leq 100$ s^{-1}	
$k_7/K_3 = 65 \pm 8$ s^{-1}	$k_7 = (9.1 \pm 1.1) \times 10^6$ M^{-1} s^{-1}
$k_8 \leq 1 \times 10^4$ M^{-1} s^{-1}	

TABLE 6: Summary of Directly Measured and Derived Results from k_B Dependence on pH at $[S_2O_8^{2-}] = 2$ mM and Constant Cl^- Molar Concentration

directly measured results	derived results
$k_4[H_2O]/K_3 = 1.1 \pm 0.1$ M s^{-1}	$k_4[H_2O] = (1.5 \pm 0.1) \times 10^5$ s^{-1}
$k_7[S_2O_8^{2-}]/K_3 = 0.12 \pm 0.01$ M s^{-1}	$k_7 = (8.4 \pm 0.7) \times 10^6$ M^{-1} s^{-1}
$k_{5'}/k_{-4} = (1.0 \pm 0.8) \times 10^{-5}$ M	$k_{5'} = (2.7 \pm 2.2) \times 10^5$ s^{-1}

Rate constant k_x is given by $k_x = k_{5a}[Cl^-] + k_{5b}[Cl] + k_{5c}[SO_4^{-\bullet}] + k_{5d}[S_2O_8^{2-}] + k_{5'}$. When the third fitting parameter is plotted as a function of Cl^- molar concentration, no dependence is observed. Therefore, it is concluded that reaction 5a is not important. The importance of reactions 5b, 5c, and 5d cannot be determined by the present data analysis. Assuming

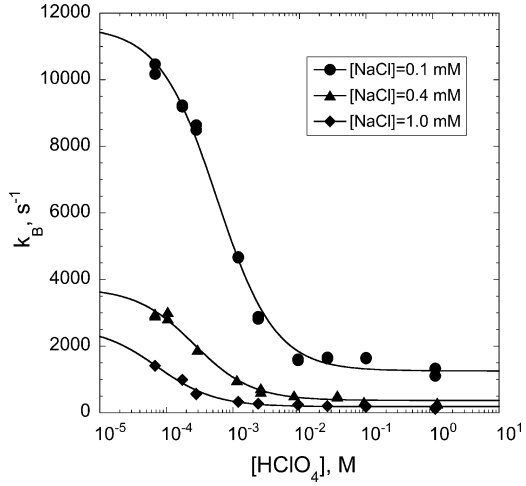

Figure 9. The k_B dependence on $[H^+]$. The solid lines are nonlinear least-squares fits by eq VIII. The circle is 0.1 mM NaCl, triangle 0.4 mM NaCl, and diamond 1.0 mM NaCl. The error bars ($\pm 1\sigma$) are usually approximately the size of or smaller than the markers.

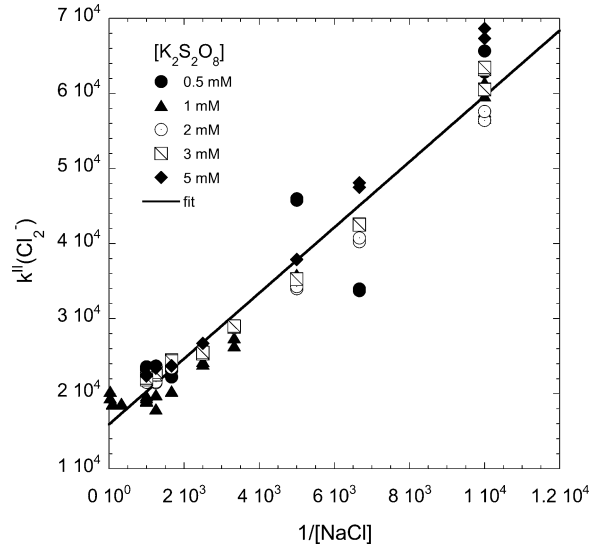

Figure 10. The dependence of $k^{II}_{Cl_2^-}$ on [NaCl]. The solid line is global linear least-squares fit. The filled circle is 0.5 mM $K_2S_2O_8$, triangle 1.0 mM $K_2S_2O_8$, open circle 2.0 mM $K_2S_2O_8$, open square 3.0 mM $K_2S_2O_8$, and diamond 5.0 mM $K_2S_2O_8$. The error bars ($\pm 1\sigma$) are usually approximately the size of or smaller than the markers.

that these three reactions are much slower than reaction 5′, k_x is equal to $k_{5'}$ and we obtain $k_{5'} = (2.7 \pm 2.2) \times 10^5$ s^{-1}.[11]

Second-Order Reaction. When the chloride concentration is relatively high, $Cl_2^{-\bullet}$ molar concentration is relatively large and the second-order contribution to the overall loss of $Cl_2^{-\bullet}$ becomes more important. Most previous studies of the second-order decay of $Cl_2^{-\bullet}$ are focused on reaction 9.[9,17,19,20,23,58,62,66,73,79,82,100−106] We find that $k^{II}_{Cl_2^-\bullet}$ varies as Cl^- molar concentration changes. When equilibrium 3 is maintained, reaction 10 is assumed to be important. Free radicals $Cl_2^{-\bullet}$ and $Cl^\bullet$ are in equilibrium with $Cl_3^{-\bullet}$, which subsequently dissociates into Cl^- and Cl_2.[54,75−77] The expression for $k^{II}_{Cl_2^-\bullet}$ is given by eq IX (derived in Appendix B).

$$k^{II}_{Cl_2^-\bullet} = \left(2k_9 + \frac{4k_{10}}{K_3[Cl^-]}\right)/\epsilon_{Cl_2^-\bullet} \qquad \text{(IX)}$$

Rate constant $k^{II}_{Cl_2^-\bullet}$ is observed to depend on Cl^- molar concentration at constant pH, as shown in Figure 10. The Debye−Hückel theory does not provide a good description of the observed behavior.

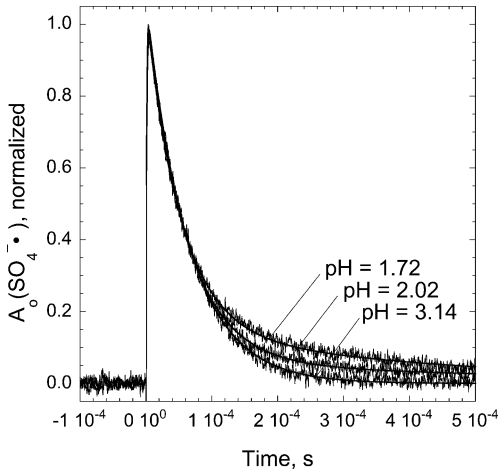

Figure 11. Some typical time profiles of $SO_4^{-\bullet}$ under various pH conditions. The solid lines are nonlinear least-squares fits. The pH of solutions is controlled by adding $HClO_4$. The experimental conditions are $[NaCl] = 4 \times 10^{-4}$ M and $[K_2S_2O_8] = 2 \times 10^{-3}$ M.

4.3.4. $SO_4^{-\bullet}$ Analysis. Some typical time profiles of $SO_4^{-\bullet}$ absorption observed at 450 nm under various conditions are shown in Figure 11. Equation X for mixed first- and second-order kinetics[19,41] was used in a nonlinear least-squares analysis to obtain the rate constants.

$$A(t)_x = \epsilon_{SO_4^-\bullet} s[SO_4^{-\bullet}] = \left\{\exp(k^I t)\left[\frac{1}{A_0} + \frac{2k_{11}}{\epsilon_{SO_4^-\bullet} s k^I}\right] - \frac{2k_{11}}{\epsilon_{SO_4^-\bullet} s k^I}\right\}^{-1} \qquad \text{(X)}$$

The rise of $SO_4^{-\bullet}$ molar concentration is faster than the instrument response. The pseudo-first-order component of the mixed kinetics is due to reactions 2, 12, and 13, and the second-order component is due to reaction 11, that is, $k^I_{SO_4^-\bullet} = k_2[Cl^-] + k_{12}[S_2O_8^{2-}] + k_{13}[H_2O]$ and $k^{II} = 2k_{11}/\epsilon_{SO_4^-\bullet}$.

Several rate constants are obtained from the analysis of the pseudo-first-order component of the $SO_4^{-\bullet}$ decay. A plot of $k^I_{SO_4^-\bullet}$ vs $[Cl^-]$ at constant pH and $S_2O_8^{2-}$ molar concentration is shown in Figure 12. The slope obtained from the linear least-squares fit corresponds to k_2, and the intercept corresponds to $k_{12}[S_2O_8^{2-}] + k_{13}[H_2O]$. The value of k_{11} is obtained directly from the mixed first- and second-order analysis, and the results are reported in Table 7.

5. Discussion

5.1. Ionic Strength Effects. Rate constants for reactions taking place in the aqueous phase are affected by the ionic strength of the medium. The Debye−Hückel−Bronsted−Davies semiempirical theory[41,107−110] gives a good description of many ionic strength effects:

$$\log_{10}\frac{k_\mu}{k_0} = 2Z_1Z_2A\left\{\frac{\mu^{1/2}}{1+\mu^{1/2}}\right\} - b\mu \qquad \text{(XI)}$$

where k_μ and k_0 are the rate constants at ionic strength μ and 0, respectively, Z_1 and Z_2 are the ion charges, A is the Debye−Hückel constant ($A = 0.509$ for water at 298 K), and b is an empirical constant in the range ∼0.2−0.3 for the few systems for which it has been measured.[109,110]

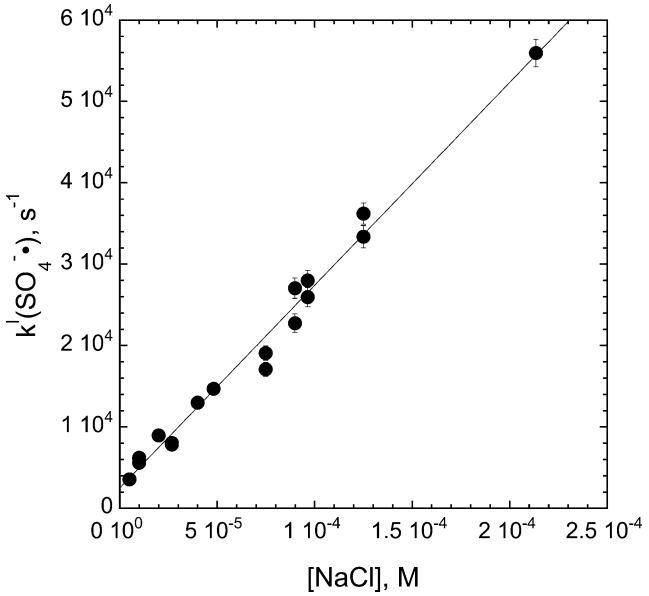

Figure 12. The $k^{I}_{SO_4^{-\bullet}}$ dependence on $[Cl^-]$ at constant pH and $[S_2O_8^{2-}]$. The solid line is linear least-squares fit. The pH is 2 by adding $HClO_4$; $[K_2S_2O_8] = 2 \times 10^{-3}$ M. The error bars ($\pm 1\sigma$) are usually approximately the size of or smaller than the markers.

Rate constants in the limit of low ionic strength were estimated by using eq XI with $b = 0$: $k_2^0 = (2.65 \pm 0.16) \times 10^8$ M^{-1} s^{-1} (from the $Cl_2^{-\bullet}$ analysis), $k_{11}^0 = (4.9 \pm 0.1) \times 10^7$ M^{-1} s^{-1}, and $k_{12}^0 = (3.5 \pm 0.2) \times 10^5$ M^{-1} s^{-1}. Rate constant k_{-4} is discussed in Paper I.[9] Since almost all of the present experiments were carried out with [NaCl] < 1 mM and pH = 2, the ionic strength of the solutions (~0.01 M) did not vary significantly. Except for reactions 2 and 9, the reaction rate constants are not affected significantly by the ionic strength, because the corresponding reactants do not include two ions.

The effect of ionic strength on k_2 and k_9 was investigated systematically by carrying out experiments of varying ionic strength up to 0.25 and 1 M, respectively, by adding $NaClO_4$. Plots of k_2 and k_9 vs $\mu^{1/2}/(1 + \mu^{1/2})$ at 296 K are presented in Figure 13a,b. The ionic strength dependence of k_2 agrees well with the Debye−Hückel theory prediction, whereas the ionic strength dependence of k_9 deviates from it.

A comparison of the present findings with those by Huie et al.[20] and McElroy[19] is shown in Figure 13b. Although all three investigations were carried out with care, there is little agreement among them regarding either the magnitudes of the rate constants or how they depend on ionic strength. The reason for this striking lack of agreement is not known, but we speculate that it may be due to trace impurities present at varying concentrations in different batches of the reagent $NaClO_4$ used to control the ionic strength. This lack of agreement and the wide range of k_9 values reported in the literature show that more work is needed.

5.2. Temperature Effects. Most of the previous measurements of k_9 were carried out at room temperature. In the present work, the temperature dependence of k_9 was investigated over the range from 6.8 to 51.6 °C, as shown in Figure 14. The solid line is a nonlinear least-squares fit to the Arrhenius expression:

$$k_9 = (5.6 \pm 0.5) \times 10^{12} \exp(-16.5 \pm 0.2 \text{ kJ mol}^{-1}/(RT))\ M^{-1}\ s^{-1} \quad \text{(XII)}$$

The $Cl_2^{-\bullet}$ disproportionation reaction 9 is exothermic ($\Delta G = -32.1$ kJ mol^{-1}), and therefore, the activation energy indicates the influence of an energy barrier. This is reasonable because both reactants are negatively charged and energy is needed to overcome the Coulombic potential and bring them from infinity to the distance corresponding to the activated complex.

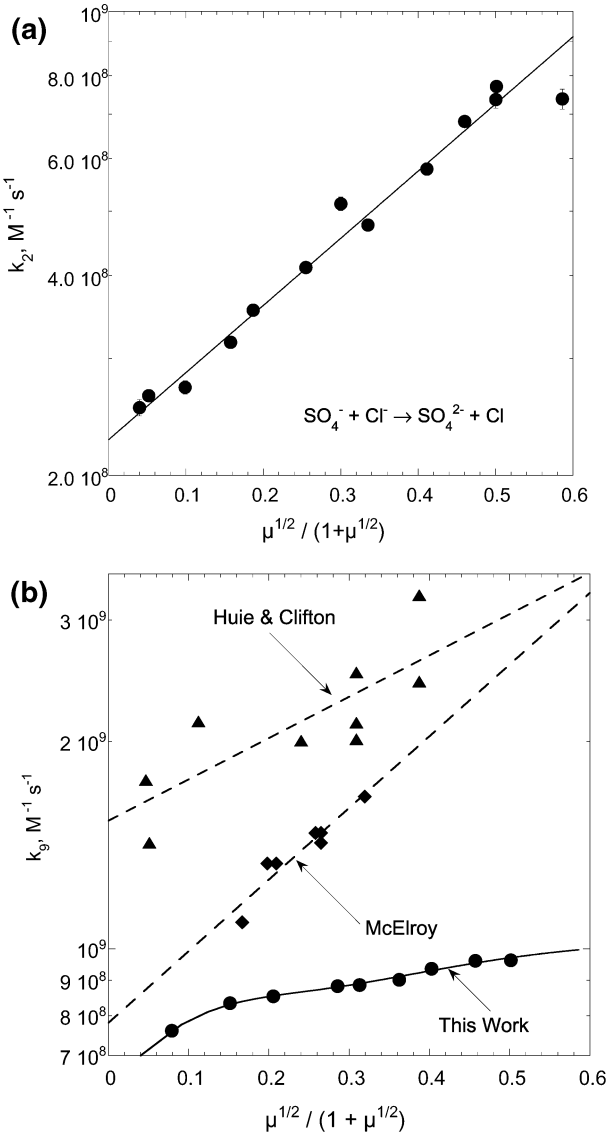

Figure 13. The ionic strength dependence (a) of k_2 at 296 K. The solid line is the linear least-squares fit to the Debye−Hückel equation. The error bars ($\pm 1\sigma$) are usually approximately the size of or smaller than the markers. Panel b shows the comparison of ionic strength dependence of k_9 data reported by Huie et al. (▲), McElroy et al. (◆) and this work (●). The dotted lines are least-squares fits of the experimental data to the Debye−Hückel equation with the slope as an adjustable parameter. The solid line is a nonlinear least-squares fit using an ion-pair model.[23]

5.3. Rate Constant Values. We determined a series of rate constants and rate constant to equilibrium constant ratios from the above kinetics analyses. In the following, we compare our experimental results with previous literature values. The comparison and discussion are arranged in the order of how the rate constants were determined, that is, from $Cl_2^{-\bullet}$ first-order, $Cl_2^{-\bullet}$ second-order, $SO_4^{-\bullet}$ first-order, and $SO_4^{-\bullet}$ second-order analyses. When the rate constants are determined from two different approaches, both results are discussed together. Since critical reviews of the relevant kinetics data are lacking, we have assembled tables of the most relevant measurements.

5.3.1. Rate Constant k_2. Several methods have been used to determine k_2. The first method is to monitor and analyze the

TABLE 7: Summary of Directly Measured and Derived Results from Analysis of the $SO_4^{-\bullet}$ Decay by Mixed First- and Second-Order Decay

source	method	parameter	directly measured results	derived results
first-order	$k^I_{SO_4^-}$−[Cl^-] linear fit	slope	$k_2 = (3.1 \pm 0.1) \times 10^8\ M^{-1}\ s^{-1}$	
		intercept	$k_{12}[S_2O_8^{2-}] + k_{13}[H_2O] = (2.1 \pm 0.1) \times 10^3\ s^{-1}$	
first-order			$k_{13}[H_2O] = 460 \pm 90\ s^{-1}$	$k_{12} = (5.5 \pm 0.3) \times 10^5\ M^{-1}\ s^{-1}$
second-order			$2k_{11}/\epsilon_{SO_4^-} = (7.7 \pm 0.2) \times 10^5\ cm\ s^{-1}$	$k_{11} = (6.1 \pm 0.15) \times 10^8\ M^{-1}\ s^{-1}$

TABLE 8: Comparison of k_2, $SO_4^{-\bullet} + Cl^- \rightarrow SO_4^{2-} + Cl^\bullet$, Determined at Room Temperature

method[a]	species	I, M[b]	k_2, $\times 10^{-8}\ M^{-1}\ s^{-1}$	reference
FP	RNO		very low	1970[14]
PR	$SO_4^{-\bullet}$	0.195	2.0 ± 0.4	1986[17]
FP−ESR	$SO_4^{-\bullet}$	0.007	3.1	1975[15]
FP	$SO_4^{-\bullet}$	→0	2.6	1989[18]
FP	$SO_4^{-\bullet}$	→0	2.47 ± 0.09	1990[20]
FP	$SO_4^{-\bullet}$	0.1	4.7	1991[21]
FP	$SO_4^{-\bullet}$	→0	3.3 ± 0.5	1996[22]
FP	$SO_4^{-\bullet}$	→0	2.49 ± 0.06	1997[23]
FP	$SO_4^{-\bullet}$	→0	2.49 ± 0.08	this work, 2003
PR	$Cl_2^{-\bullet}$	5.05	4.1	1976[89]
PR	$Cl_2^{-\bullet}$	0.056	1.3	1976[16,89]
FP	$Cl_2^{-\bullet}$	→0	2.7 ± 0.4	1990[19]
FP	$Cl_2^{-\bullet}$	→0	3.0 ± 0.9	1996[22]
FP	$Cl_2^{-\bullet}$	→0	2.65 ± 0.16	this work, 2003
FP	$SO_4^{-\bullet}$ and $Cl_2^{-\bullet}$	0.3	6.1 ± 0.2	1999[24]
FP	$SO_4^{-\bullet}$ and $Cl_2^{-\bullet}$	→0	2.47	1999[24]

[a] PR, pulse radiolysis; FP, flash photolysis; ESR, electron spin resonance. [b] →0: ionic strength is extrapolated to 0 M.

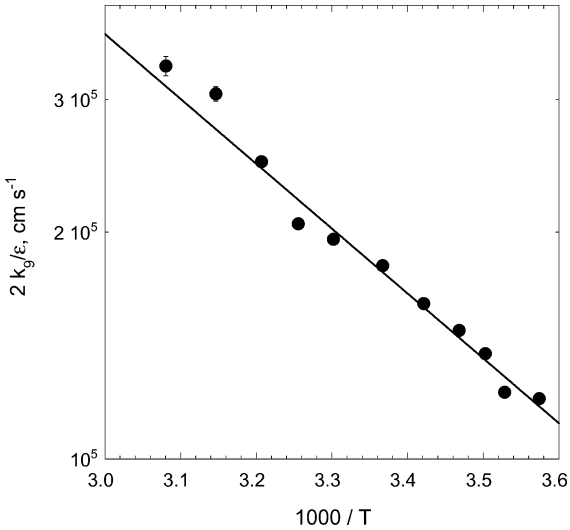

Figure 14. The Arrhenius plot of k_9 (points) and nonlinear least-squares fit (line). The error bars (±1σ) are usually approximately the size of or smaller than the markers.

$SO_4^{-\bullet}$ decay, the second is to analyze the $Cl_2^{-\bullet}$ rise, and the third is to combine the first two methods. The value of $k_2 = (3.1 \pm 0.1) \times 10^8\ M^{-1}\ s^{-1}$ obtained from $SO_4^{-\bullet}$ decay analysis is consistent within error limits with that from the $Cl_2^{-\bullet}$ molar concentration growth analysis in this work. The unweighted average of the above two results, $k_2 = (3.2 \pm 0.2) \times 10^8\ M^{-1}\ s^{-1}$, is reported in Table 1. Despite differences in analytical methods, the present results are in agreement with previous measurements (see Table 8).[14−24,43,81,89,93−95]

Herrmann et al.[22] presented their self-consistent results from the decay of $SO_4^{-\bullet}$ and the growth of $Cl_2^{-\bullet}$. Buxton et al.[24] added SO_4^{2-} to the system of $SO_4^{-\bullet}$ and Cl^- to study equilibrium 2. Both k_2 and k_{-2} were obtained by analyzing the $SO_4^{-\bullet}$ decay and $Cl_2^{-\bullet}$ growth. The higher value of k_2 by Buxton et al. may be caused by the ionic strength of 0.3 M used in their experiment. Using Debye−Hückel theory,[41,107−110] we extrapolated Buxton et al.'s result to infinite dilution, where it is found to be in excellent agreement with our results at zero ionic strength (Table 1).

5.3.2. Rate Constants from First-Order $Cl_2^{-\bullet}$ Decay. Two values for the ratio $k_4[H_2O]/K_3$ were obtained: 1.2 ± 0.1 and 1.1 ± 0.1 M s^{-1} from k_B vs [Cl^-] and [$S_2O_8^{2-}$] and k_B vs pH, respectively. These results are also reasonably consistent with the value 1.4 ± 0.1 M s^{-1} from Paper I.[9,72] With the recommended value of $K_3 = (1.4 \pm 0.2) \times 10^5\ M^{-1}$, two values for $k_4[H_2O]$ are obtained: $(1.7 \pm 0.1) \times 10^5\ s^{-1}$ and $(1.5 \pm 0.1) \times 10^5\ s^{-1}$. The unweighted average of these two values is consistent with literature values[9,19,60,72,81,96] and reported in Table 1 as $k_4[H_2O]$.

McElroy[19] pointed out that when $[Cl_2^{-\bullet}]/[Cl^\bullet] \geq 10$, the absorption due to $Cl^\bullet$ atoms is negligible compared to that due to $Cl_2^{-\bullet}$, considering $K_3 = (1.4 \pm 0.2) \times 10^5\ M^{-1}$ (Paper I[9]), $\epsilon_{Cl_2^-,364nm} = 7000\ M^{-1}\ cm^{-1}$, $\epsilon_{Cl^\bullet,364nm} \approx 3000\ M^{-1}\ cm^{-1}$,[63,85] and $\epsilon_{ClOH^{-\bullet},364nm} \approx 3200\ M^{-1}\ cm^{-1}$.[60] The contribution of $ClOH^{-\bullet}$ is also expected to be minimal. At high Cl^- molar concentration, an equilibrium between dichloride anion radicals and chlorine atoms is rapidly achieved. Based upon reactions $Cl^\bullet + H_2O \leftrightarrow HOClH$ and $HOClH \leftrightarrow ClOH^{-\bullet} + H^+$ postulated by Buxton et al.[111] (essentially reactions 4 and −4 in Table 1), the first-order rate constant for Cl^- decay should show an inverse dependence on the chloride ion concentration due to reactions 3 and 4. The observed first-order decay rate constant k_B was found to increase markedly when [Cl^-] < 1 mM; rate constant k_B reaches a lower limit at [Cl^-] = 0.01 M. However, k_B is not proportional to $[Cl^-]^{-1}$. Later, Jacobi et al.[81] found $k_B \propto [Cl^-]^{-1}$ in experiments with [Cl^-] > 0.3 mM. In the present work, $k_B \propto [Cl^-]^{-1}$ is found over a relatively wide range of $[Cl^-] \geq 0.1$ mM corresponding to $[Cl^\bullet] \ll [Cl_2^{-\bullet}]$ and $K_3[Cl^-] \gg 1$.

Although it had been proposed[19,111] that k_B should be dependent on pH due to equilibrium 4, previous experimental data showed inconsistent results.[19,82,111] Wagner et al.[82] did not include reaction −4 in their $Cl_2^{-\bullet}$ mechanism. In deaerated solutions at high pH, the decrease in conductivity due to the difference in mobility of the electron and the $Cl_2^{-\bullet}$ may have been too small to detect with their equipment,[82] which may explain why they did not observe a pH dependence.

McElroy[19] attributed reactions −3, 4, and 5 to the $Cl_2^{-\bullet}$ decay, and described the overall process by reaction 15.

$$Cl_2^{-\bullet} + H_2O \leftrightarrow H^+ + 2Cl^- + HO^\bullet \qquad (15)$$

The equilibrium $Cl^\bullet + H_2O \leftrightarrow H_2OCl$ was postulated to explain the lack of the pH dependence on the decay rate of $Cl^\bullet/Cl_2^{-\bullet}$ over the pH range of 2.2−3.9. Since McElroy used HCl to control the pH,[19] it is likely that the combined effects of Cl^- and H^+ molar concentrations on k_B confounded the interpretation.

Buxton et al.[111] used photolysis of CH_3COCH_2Cl to generate $Cl^\bullet$, which subsequently reacts with Cl^- to form $Cl_2^{-\bullet}$. The reactions of $Cl^\bullet$ with water and chloroacetone in the pH range

TABLE 9: Comparison of k_9, $Cl_2^{-\bullet} + Cl_2^{-\bullet} \rightarrow 2Cl^- + Cl_2$, Determined at Room Temperature

k_9, $\times 10^{-9}$ M^{-1} s^{-1}	I, M	$(2k_9/\epsilon)$, $\times 10^{-5}$ cm s^{-1}	$\epsilon(Cl_2^{-\bullet})$, M^{-1} cm^{-1}	λ, nm	method[a]	reference
5.5 ± 3.5	0.25	8.8 ± 5.6	12500	340	LFP	1989[32,50]
1.3	0	2.96	8800	340	LFP	1990[20]
0.7 ± 0.1	0	1.6	8800	340	LFP	1990[19]
1.55 ± 0.05	0.13	3.65 ± 0.12	8800	340	PR	1990[19]
0.69 ± 0.005	0	1.57 ± 0.11	8800	340	LFP	1997[23]
1.8 ± 0.1	0	4.24 ± 0.24	8300	325	LFP	1999[73]
0.61	0		9600	340	FP	2000[112]
2.0 ± 0.3	<1	4.55 ± 0.76	8800	340	PR	2003[91]
0.9 ± 0.05	$<10^4$	2.54 ± 0.16	7000	364	LFP	this work and 2003[9]
0.72 ± 0.08	0	2.06 ± 0.27	7000	364	LFP	this work, 2003

[a] PR, pulse radiolysis; LFP, laser flash photolysis.

TABLE 10: Comparison of k_{11}, $SO_4^{-\bullet} + SO_4^{-\bullet} \rightarrow S_2O_8^{2-}$, Determined at Room Temperature

method[a]	I, M	λ, nm	$\epsilon_{SO_4^-}$, cm^{-1} M^{-1}	$2k_{11}/\epsilon_{SO_4^-}$, $\times 10^{-5}$ cm s^{-1}	k_{11}, $\times 10^{-8}$ M^{-1} s^{-1}	reference
PR	4	450	450	36	8.1	1987[122]
PR	concd	450	1600	4.75	3.8 ± 0.5	1992[40]
FP	0.06	455	450 ± 45	18.6[b]	4.2[b]	1967[34]
FP	0.03	455	460 ± 25	8.0 ± 0.7[b]	3.7 ± 0.3[b,c]	1967[29]
FP	~3				6.1 ± 1.1[b,c]	1967[35]
FP	12	450	1050	6.05[e]	18	1973[113]
FP	0.03, 0.13, 1	450	460	7.74[c]	1.78	1977[123]
FP	*d*	*d*	*d*	*d*	2.5	1978[124]
FP	0	450	1385 ± 140	3.9 ± 0.6	2.7	1988[37]
FP	0	450	1600	5.5	4.45 ± 0.15	1990[39]
FP	1.5×10^{-4}	450	1385	3.2	2.2 ± 0.15	1993[52]
FP	*d*	*d*	*d*	*d*	0.55	1993[116]
FP	$\leq 1.5 \times 10^{-4}$	*d*	*d*	*d*	1.6[b]	1995[114]
FP	$\gg 0$	454	*d*	2.5 ± 0.2	*d*	1996[41]
FP	≤ 0.25	450	1630 ± 10	7.7 ± 0.2	6.1 ± 0.15	this work, 2003

[a] PR, pulse radiolysis; FP, flash photolysis [b] Original reported as $k_{11}/\epsilon_{SO_4^-}$ or k_{11}. [c] Averaged results of measurements reported in the same paper. [d] Not available. [e] Based on 2.38 cm path length.

1−6 were studied, where pH was adjusted by addition of either $HClO_4$ or NaOH. Little dependence of k_B on H^+ molar concentration was observed. Buxton et al.[111] also disagreed with McElroy[19] about the necessity of using the equilibrium of $Cl^{\bullet} + H_2O \leftrightarrow H_2OCl$, because their calculations suggested that $Cl^{\bullet}$ and H_2OCl are not different species. Although not discussed, many possible radical reactions could be involved in the system studied by Buxton et al. For example, the products produced by $Cl^{\bullet}$ reacting with CH_3COCH_2Cl were not identified. More research is needed to determine the possible factors in the photolysis of chloroacetone that may affect the pH dependence.

Reaction 6 is slow, as concluded elsewhere.[9,19,72,81,82] The value $k_6[H_2O] < 100$ s^{-1} is determined in the present work directly from k_B vs $[S_2O_8^{2-}]$ and $1/[Cl^-]$ analyses, in agreement with previous measurements.[9,19,60,72,81,96]

As shown in the data analysis section, k_B depends not only on Cl^- molar concentration, but also on $S_2O_8^{2-}$ molar concentration via reactions 7 and 8. Here, values of k_7 and k_8 are reported for the first time. Buxton et al. carried out pulse radiolysis experiments on a system containing *tert*-butyl alcohol, $[Cl^-] = 10^{-3}$ M, and $[S_2O_8^{2-}] \leq 0.1$ M but did not detect these reactions,[72] possibly because reaction 7 is not very important at this chloride concentration and reaction 8 is very slow. The value $k_7 = (9.1 \pm 0.1) \times 10^6$ M^{-1} s^{-1} is obtained on the basis of $K_3 = 1.4 \times 10^5$ M^{-1}.[9,72] Since the fitting uncertainty of k_8 is quite large, only a limiting value is obtained: $k_8 < 1 \times 10^4$ M^{-1} s^{-1}. Reaction 7 is relatively fast, possibly due to the high reactivity of $Cl^{\bullet}$ in the aqueous phase. The possible products of reactions 7 and 8 include $ClSO_4^-$, $SO_4^{-\bullet}$, and SO_4^{2-}. We speculate that the structure of $ClSO_4^-$ is similar to that of $SO_4^{-\bullet}$ except that one terminal oxygen in the $SO_4^{-\bullet}$ tetrahedron is bonded to a $Cl^{\bullet}$ atom. More research is needed to determine the products of reactions 7 and 8.

The ratio $k_7[S_2O_8^{2-}]/K_3 = (0.12 \pm 0.01)$ M^{-1} s^{-1} is directly obtained from the analysis of pH dependence of k_B at $[S_2O_8^{2-}] = 2$ mM. The value $k_7 = (8.4 \pm 0.7) \times 10^6$ M^{-1} s^{-1} is derived on the basis of $K_3 = 1.4 \times 10^5$ M^{-1},[9,72] and it is consistent with that obtained from the k_B vs $1/[Cl^-]$ analysis in this work. The unweighted average of these two values is reported in Table 1.

5.3.3. Rate Constants from $Cl_2^{-\bullet}$ Second-Order Analysis. Recent values of k_9 obtained from this and previous[9,19,20,23,32,73,91,112] work are summarized in Table 9. Our result is consistent with the most recent measurements. The parameter determined directly by experiments is $2k_9/\epsilon_{Cl_2^-}$. The final result for k_9 depends on the value of $\epsilon_{Cl_2^-\bullet}$. Reaction 10 is quite fast, which is consistent with the previous result by Wu et al.[79]

5.3.4. Rate Constants from $SO_4^{-\bullet}$ First-Order Analysis. The second-order component of $SO_4^{-\bullet}$ decay is obtained directly from the mixed first- and second-order analysis of $SO_4^{-\bullet}$. The values of k_{11} are listed in Table 10. The experimentally measured quantity is $2k_{11}/\epsilon_{SO_4^-\bullet}$; thus $\epsilon_{SO_4^-\bullet}$ affects the deduced k_{11}. As shown in Table 10, our result is consistent with the many previous measurements of $2k_{11}/\epsilon_{SO_4^-\bullet}$.[18,24,29,34−44,52,94,113,114] It is found in this work that $2k_{11}/\epsilon_{SO_4^-\bullet}$ is affected by ionic strength.[37,39,41] The value reported here is higher than a previous measurement in this laboratory[41] obtained at almost zero ionic strength. Our present result is in good agreement with Tang et al.[37] obtained at a similar ionic strength. The recommendation for k_{11}^0 extrapolated to zero ionic strength is listed in Table 13.

5.3.5. Second-Order Rate Constants from $SO_4^{-\bullet}$ Analysis. Table 11 summarizes values for k_{12}, which fall into two distinct

TABLE 11: Comparison of k_{12}, $SO_4^{-\bullet} + S_2O_8^{2-} \rightarrow SO_4^{2-} + S_2O_8^{-\bullet}$, Determined at Room Temperature

method[a]	*I*, M	k_{12}, M^{-1} s^{-1}	reference
PR	*b*	1.2×10^6	1987[122]
FP	3×10^{-3}	$(6.1 \pm 0.6) \times 10^5$	1990[39]
PR	concd[c]	$(6.6 \pm 2.7) \times 10^5$	1992[40]
FP	*b*	$\leq 5 \times 10^5$	1994[94]
FP	$(0.5-5) \times 10^{-4}$	$(6.6 \pm 0.4) \times 10^5$	1995[114]
FP	*b*	6.3×10^5	1996[42]
FP	≤ 0.25	$(5.5 \pm 0.3) \times 10^5$	this work, 2003
PR	≤ 0.12	not observed	1988[37]
FP	0.28−6.1	$\leq 10^4$	1997[41]
FP	$(3 \times 10^{-4})-3$	slow	1999[115]
FP	0.3	<1500	1999[24]
FP	≤ 0.25	580 ± 90	this work, 2003

[a] PR, pulse radiolysis; FP, flash photolysis. [b] Not available. [c] concd, concentrated H_2SO_4.

TABLE 12: Comparison of k_{13}, $SO_4^{-\bullet} + H_2O \rightarrow HO^\bullet + HSO_4^-$, Determined at Room Temperature[a]

method	*I*, M	pH	$k_{13}[H_2O]$, s^{-1}	reference
PR	NA	>7	<3000	1972[36]
PR	0.3	~6	690 ± 120	1999[24]
FP	$\sim 3 \times 10^3$	1.5−5.4	410 ± 40[b]	1988[37]
FP	$\sim 3 \times 10^3$	1.5−5.4	360 ± 90[c]	1988[37]
FP	→0[d]	4.9	500 ± 60	1990[39]
FP	→0[d]	5.0	660 ± 40	1995[114]
FP	NA	NA	660	1996[42]
FP	0.28−6.1	4.8−5.8	440 ± 50	1997[41]
FP	≤ 0.25	2−5	460 ± 90	this work, 2003

[a] NA, not available; PR, pulse radiolysis; FP, flash photolysis. [b] In the absence of large concentrations of additives, H_2SO_4, $HClO_4$, $NaClO_4$, or HAc. [c] Assuming the first-order component from reactions is 50 ± 50 s^{-1}. [d] →0: Ionic strength is extrapolated to 0 M.

groups. One is in the range of 10^5 M^{-1} s^{-1},[39,40,42,94,114] and the other is about an order of magnitude lower.[24,37,41,115,116] In the present work, we obtain values that fall in both groups, raising an interesting question about k_{12}.

The high value of k_{12} obtained in this work corresponds to pH = 2, controlled by the addition of $HClO_4$, while the low value is obtained when the pH ≈ 4. This suggests that the apparent pH dependence of k_{12} may be due to contributions from reaction 14, in addition to reactions 2, 12, −12, and 13. More work is needed to identify the source of this behavior.

The value of k_{13} has been determined several times in the past.[36,37,39−41,114] In this work, laser flash photolysis of solutions containing $S_2O_8^{2-}$ with or without pH control give $k_{13}[H_2O] = 460 \pm 90$ s^{-1}. Our value for k_{13} is compared with previous determinations in Table 12. All of the measurements indicate that reaction 13 is slow.

6. Conclusions

The present work results in a more complete, self-consistent mechanism describing the kinetics of $Cl_2^{-\bullet}$ and $SO_4^{-\bullet}$ (see Table 1). Our results are consistent with literature values, where available, supporting the general correctness of the reaction mechanism summarized in Table 1. In addition, the absorption spectra of $SO_4^{-\bullet}$ and $Cl_2^{-\bullet}$ have been redetermined, and the results are in excellent agreement with previous work. The pseudo-first-order decay rate constant of $Cl_2^{-\bullet}$ is, for the first time, shown to depend on pH as expected from the effects of reaction −4. The temperature and ionic strength dependences of k_9 are measured, as is the ionic strength dependence of k_2. The results for k_9 show that the ionic strength dependence is still far from certain and should be the subject of future work, because application to real systems will require large corrections for ionic strength. The observed pseudo-first-order decay rate constant of $SO_4^{-\bullet}$ appears to depend on pH and further work is also needed to determine this aspect of the mechanism.

Acknowledgment. We thank NASA (Upper Atmospheric Research Program) and NSF (Atmospheric Chemistry Division) for financial support of this work. We also thank Robert Huie, Paul Wine, and Anthony Hynes for helpful discussions. (This material is based upon work supported by the National Science Foundation under Grant No. 9812680. Any opinions, findings, and conclusions or recommendations expressed in this material are those of the author(s) and do not necessarily reflect the views of the National Science Foundation.)

TABLE 13: Summary of Results and Recommendations for Rate Constants[a]

reaction	results (this paper)	recommendations	reference
1			
2	$k_2^0 = (2.57 \pm 0.11) \times 10^8$ M^{-1} s^{-1}	$k_2^0 = (2.57 \pm 0.11) \times 10^8$ M^{-1} s^{-1}	this work
−2		$k_{-2} = (2.1 \pm 0.1) \times 10^8$ M^{-1} s^{-1}	21, 24
3		$k_3 = (7.8 \pm 0.8) \times 10^9$ M^{-1} s^{-1}	9
−3		$k_{-3} = (5.3 \pm 0.3) \times 10^4$ s^{-1}	9
		$K_3 = (1.4 \pm 0.2) \times 10^5$ M^{-1}	9
4	$k_4[H_2O] = (1.6 \pm 0.2) \times 10^5$ s^{-1}	$k_4[H_2O] = (1.7 \pm 0.3) \times 10^5$ s^{-1}	this work and ref 9
−4		$k_{-4}^0 = (3.3 \pm 0.9) \times 10^{10}$ M^{-1} s^{-1}	9
		$1/K_4^0 = (8.8 \pm 2.2) \times 10^7$	this work and ref 9
5		$k_5 = (6.1 \pm 0.8) \times 10^9$ s^{-1}	60
−5		$k_{-5} = (4.3 \pm 0.4) \times 10^9$ M^{-1} s^{-1}	60
		$1/K_5 = 0.70 \pm 0.13$ M^{-1}	9
6	$k_6[H_2O] < 100$ s^{-1}	$k_6[H_2O] < 100$ s^{-1}	this work and ref 9
7	$k_7 = (8.8 \pm 0.5) \times 10^6$ M^{-1} s^{-1}	$k_7 = (8.8 \pm 0.5) \times 10^6$ M^{-1} s^{-1}	this work
8	$k_8 < 1 \times 10^4$ M^{-1} s^{-1}	$k_8 < 1 \times 10^4$ M^{-1} s^{-1}	this work
9	$k_9^0 = (7.2 \pm 0.8) \times 10^8$ M^{-1} s^{-1}	$k_9^0 = (7.2 \pm 0.8) \times 10^8$ M^{-1} s^{-1}	this work and ref 9
10	$k_{10} = (2.1 \pm 0.1) \times 10^9$ M^{-1} s^{-1}	$k_{10} = (2.1 \pm 0.1) \times 10^9$ M^{-1} s^{-1}	this work
11	$k_{11}^0 = (4.91 \pm 0.08) \times 10^8$ M^{-1} s^{-1}	$k_{11}^0 = (4.91 \pm 0.08) \times 10^8$ M^{-1} s^{-1}	this work
12	$k_{12}^0 = (3.5 \pm 0.2) \times 10^5$ M^{-1} s^{-1}	$k_{12}^0 = (3.5 \pm 0.2) \times 10^5$ M^{-1} s^{-1}	this work
13	$k_{13}[H_2O] = 460 \pm 90$ s^{-1}	$k_{13}[H_2O] = 460 \pm 90$ s^{-1}	this work and ref 41
−13		$k_{-13} = 6.9 \times 10^5$ M^{-1} s^{-1}	46
14		$K_{14} = 1.2 \times 10^{-2}$ M^{-1}	117

[a] This paper; uncertainties ($\pm 1\sigma$) were obtained from error propagation; ionic strength $\mu \approx 0.01$ M unless otherwise noted by a superscript "0" on rate constants that have been adjusted to $\mu = 0$.

Appendix A. The k_B Dependence on pH

The rate law expressions of $Cl^{\bullet}$ and $ClOH^{-\bullet}$ are

$$\frac{d[Cl^{\bullet}]}{dt} = k_2[SO_4^{-\bullet}][Cl^-] - [Cl^{\bullet}]\{k_{-2}[SO_4^{2-}] - k_3[Cl^-] + k_4[H_2O] + k_7[S_2O_8^{2-}]\} + k_{-4}[ClOH^{-\bullet}][H^+] - k_{-3}[Cl_2^{-\bullet}] \quad (A.1)$$

$$\frac{d[ClOH^{-\bullet}]}{dt} = k_4[Cl^{\bullet}][H_2O] - [ClOH^{-\bullet}](k_{-4}[H^+] + k_x) \quad (A.2)$$

where $k_x = k_{5a}[Cl^-] + k_{5b}[Cl^{\bullet}] + k_{5c}[SO_4^{-\bullet}] + k_{5d}[S_2O_8^{2-}] + k_{5'}$. Due to the presence of Cl^- in the system, k_5 is negligible. By steady-state approximation, $[ClOH^{-\bullet}]_{ss}$ is expressed as

$$[ClOH^{-\bullet}]_{ss} = \frac{k_4[Cl^{\bullet}][H_2O]}{k_{-4}[H^+] + k_x} \quad (A.3)$$

When equilibria 2 and 3 are maintained and Cl^- and $S_2O_8^{2-}$ molar concentrations are kept constant, the kinetics behavior observed is mainly caused by $Cl^{\bullet}$,

$$\frac{d[Cl^{\bullet}]}{dt} = -k[Cl^{\bullet}] = -k_B[Cl_2^{-\bullet}] \quad (A.4)$$

where

$$k = k_4[H_2O] + k_7[S_2O_8^{2-}] - \frac{k_4[H_2O]}{1 + k_x/(k_{-4}[H^+])}$$

and

$$[Cl^{\bullet}] = \frac{[Cl_2^{-\bullet}]}{K_3[Cl^-]}$$

therefore

$$k_B = \frac{k_4[H_2O] + k_7[S_2O_8^{2-}] - \dfrac{k_4[H_2O]}{1 + k_x/(k_{-4}[H^+])}}{K_3[Cl^-]} \quad (A.5)$$

Appendix B. The $k^{II}_{Cl_2^-}$ Dependence on Cl− Molar Concentration

The second-order decay of $Cl_2^{-\bullet}$ is attributed to equilibrium 3 and reactions 9 and 10. If only the second-order decay is considered, the expressions of $Cl_2^{-\bullet}$ and $Cl^{\bullet}$ are

$$\frac{d[Cl_2^{-\bullet}]}{dt} = -2k_9[Cl_2^{-\bullet}]^2 - 2k_{10}[Cl_2^{-\bullet}][Cl^{\bullet}] - k_{-3}[Cl_2^{-\bullet}] + k_3[Cl^-][Cl^{\bullet}] \quad (B.1)$$

$$\frac{d[Cl^{\bullet}]}{dt} = -k_3[Cl^-][Cl^{\bullet}] + k_{-3}[Cl_2^{-\bullet}] - 2k_{10}[Cl_2^{-\bullet}][Cl^{\bullet}] \quad (B.2)$$

The addition of eqs B.1 and B.2 generates eq B.3

$$-\left(\frac{d[Cl_2^{-\bullet}]}{dt} + \frac{d[Cl^{\bullet}]}{dt}\right) = 2k_9[Cl_2^{-\bullet}]^2 + 4k_{10}[Cl_2^{-\bullet}][Cl^{\bullet}] \quad (B.3)$$

When equilibrium 3 is maintained and $k_3[Cl^-][Cl^{\bullet}] \gg 2k_{10}[Cl_2^{-\bullet}][Cl^{\bullet}]$,

$$-\left(\frac{d[Cl_2^{-\bullet}]}{dt} + \frac{d[Cl^{\bullet}]}{dt}\right) = 2k_{Cl_2^-\bullet}[Cl_2^{-\bullet}]^2 \quad (B.4)$$

which leads to

$$k^{II}_{Cl_2^-\bullet} = \left(2k_9 + \frac{4k_{10}}{K_3[Cl^-]}\right)/\epsilon_{Cl_2^-\bullet} \quad (B.5)$$

References and Notes

(1) Graedel, T. E.; Weschler, C. J. *Rev. Geophys. Space Phys.* **1981**, *19*, 505−539.
(2) Graedel, T. E. *Atmos. Environ.* **1984**, *18*, 1835−1842.
(3) Chameides, W. L. *J. Geophys. Res.* **1986**, *91*, 5331−5337.
(4) Seinfeld, J. H. *Atmospheric Chemistry and Physics of Air Pollution*; John Wiley & Sons: New York, 1986.
(5) Faust, B. C. *Environ. Sci. Technol.* **1994**, *28*, 217A−222A.
(6) Huie, R. E. Free radical chemistry of the atmospheric aqueous phase. In *Progress and Problems in Atmospheric Chemistry*, 1st ed.; Barker, J. R., Ed.; World Scientific: Singapore, 1995; pp 374−419.
(7) Chameides, W. L.; Davis, D. D. *J. Geophys. Res.* **1982**, *87*, 4863−4877.
(8) Chameides, W. L. *J. Geophys. Res.* **1984**, *89*, 4739−4755.
(9) Yu, X.-Y.; Barker, J. R. *J. Phys. Chem. A.* **2003**, *107*, 1313−1324.
(10) Yu, X.-Y.; Barker, J. R. *J. Phys. Chem. A.* **2003**, *107*, 1325−1332.
(11) Yu, X.-Y. *J. Phys. Chem. Ref. Data*, submitted for publication, 2003.
(12) Liu, Y.; Pimentel, A. S.; Antoku, Y.; Giles, B. J.; Barker, J. R. *J. Phys. Chem. A.* **2002**, *106*, 11075−11082.
(13) Liu, Y.; Sheaffer, R. L.; Barker, J. R. *J. Phys. Chem. A* **2003**, *107*, 10296−10303.
(14) Kralji'c, I. *Int. J. Radiat. Phys. Chem.* **1970**, *59*, 59−68.
(15) Chawla, O. P.; Fessenden, R. W. *J. Phys. Chem.* **1975**, *79*, 2693−2700.
(16) Kim, K.-J.; Hamill, W. H. *J. Phys. Chem.* **1976**, *80*, 2325−2330.
(17) Slama-Schwok, A.; Rabani, J. *J. Phys. Chem.* **1986**, *90*, 1176−1179.
(18) Wine, P. H.; Tang, Y.; Thorn, T. P.; Wells, J. R. *J. Geophys. Res.* **1989**, *94*, 1085−1094.
(19) McElroy, W. J. *J. Phys. Chem.* **1990**, *94*, 2435−2441.
(20) Huie, R. E.; Clifton, C. L. *J. Phys. Chem.* **1990**, *94*, 8561−8567.
(21) Huie, R. E.; Clifton, C. L.; Neta, P. *Radiat. Phys. Chem.* **1991**, *38*, 477−481.
(22) Herrmann, H.; Jacobi, H.-W.; Reese, A.; Zellner, R. Laboratory studies of small radicals and radical anions of interest for tropospheric aqueous phase chemistry: The reactivity of SO_4^-. In *EUROTRAC Symposium '96*; Borrell, P. M., Borrell, P., Cvitas, T., Kelly, K., Seiler, W., Eds.; Springer: Berlin and New York, 1996.
(23) Bao, Z.-C. Temperature and ionic strength dependence of some sulfate [SO_4^-(aq)] and dichloride [Cl_2^-(aq)] radical reactions. Ph.D. Thesis, University of Michigan, Ann Arbor, MI, 1997.
(24) Buxton, G. V.; Bydder, M.; Salmon, G. A. *Phys. Chem. Chem. Phys.* **1999**, *1*, 269−273.
(25) Livinston, J.; Morgan, R.; Crist, R. H. *J. Am. Chem. Soc.* **1927**, *49*, 16−25.
(26) Crist, R. H. *J. Am. Chem. Soc.* **1932**, *54*, 3939−3942.
(27) Heidt, L. J. *J. Chem. Phys.* **1942**, *10*, 297−302.
(28) Tsao, M.-S.; Wilmarth, W. K. *J. Phys. Chem.* **1959**, *63*, 346−353.
(29) Dogliotti, L.; Hayon, E. *J. Phys. Chem.* **1967**, *71*, 2511−2516.
(30) de Vries, K. J.; Gellings, P. J. *J. Inorg. Nucl. Chem.* **1969**, *31*, 1307−1313.
(31) Radtsig, V. A.; Politov, A. A. *Kinet. Catal. (Inst. Chem. Phys., Acad. Sci. USSR)* **1984**, *26*, 42−50 (original); 33−40 (English translation).
(32) Hynes, A. J.; Wine, P. H. *J. Chem. Phys.* **1988**, *89*, 3565−3572.
(33) Evans, R. C. *Crystal Chemistry*; Cambridge University Press: New York, 1939.
(34) Hayon, E.; McGarvey, J. J. *J. Phys. Chem.* **1967**, *71*, 1472−1477.
(35) Dogliotti, L.; Hayon, E. *J. Phys. Chem.* **1967**, *71*, 3802−3808.
(36) Hayon, E.; Treinin, A.; Wilf, J. *J. Am. Chem. Soc.* **1972**, *94*, 47−57.
(37) Tang, Y.; Thorn, R. P.; Mauldin, R. L.; Wine, P. H. *J. Photochem. Photobiol., A: Chem.* **1988**, *44*, 243−258.
(38) Huie, R. E.; Clifton, C. L.; Altstein, N. *Radiat. Phys. Chem.* **1989**, *33*, 361−370.
(39) McElroy, W. J.; Waygood, S. J. *J. Chem. Soc., Farday Trans.* **1990**, *86*, 2557−2564.
(40) Jiang, P.-Y.; Katsumura, Y.; Nagaishi, R.; Domae, M.; Ishikawa, K.; Ishigure, K.; Yoshida, Y. *J. Chem. Soc., Farday Trans.* **1992**, *88*, 1653−1658.

(41) Bao, Z.-C.; Barker, J. R. *J. Phys. Chem.* **1996**, *100*, 9780−9787.
(42) Brandt, C.; Berndt, T.; Rolle, W.; Herrmann, H.; Jacobi, H.-W.; Reese, A.; Zellner, R. On the mechanism and atmospheric relevance of the iron(II)-catalysed oxidation of benzene by peroxodisulfate. In *EUROTRAC Symposium '96*; Borrell, P. M., Borrell, P., Cvitas, T., Kelly, K., Seiler, W., Eds.; Springer: Berlin and New York, 1996.
(43) Huie, R. E.; Sieck, L. W. SOx Radical Monoanions−Reactions in Solution and in the Gas Phase. In *S-Centered Radicals*, 1st ed.; Alfassi, Z. B., Ed.; John Wiley & Sons Ltd.: Chichester, England, 1999; pp 63−95.
(44) Buxton, G. V.; Salmon, G. A.; Williams, J. E. *J. Atmos. Chem.* **2000**, *36*, 111−134.
(45) Buck, R. P.; Singhadeja, S.; Rogers, L. B. *Anal. Chem.* **1954**, *26*, 1240−1242.
(46) Heckel, E.; Henglein, A.; Beck, G. *Ber. Bunsen-Ges. Phys. Chem.* **1966**, *70*, 149−154.
(47) Roebke, M.; Renz, M.; Henglein, A. *Int. J. Radiat. Phys. Chem.* **1969**, *1*, 39−44.
(48) Redpath, J. L.; Willson, R. L. *Int. J. Radiat. Biol.* **1975**, *27*, 389−398.
(49) Levine, J. S. *The Photochemistry of Atmospheres. Earth, the Other Planets, and Comets*; Academic Press: Orlando, San Diego, New York, London, Toronto, Montreal, Sydney, Tokyo, 1985.
(50) Wine, P. H.; Mauldin, R. L., III; Thorn, R. P. *J. Phys. Chem.* **1988**, *92*, 1156−1162.
(51) Kläning, U. K.; Sehested, K.; Appelman, E. H. *Inorg. Chem.* **1991**, *30*, 3582−3584.
(52) Huie, R. E.; Clifton, C. L. *Chem. Phys. Lett.* **1993**, *205*, 163−167.
(53) Buxton, G. V.; McGowan, S.; Salmon, G. A.; Williams, J. E.; Wood, N. D. *Atmos. Environ.* **1996**, *30*, 2483−2493.
(54) Zimmerman, G.; Strong, F. C. *J. Am. Chem. Soc.* **1957**, *79*, 2063−2066.
(55) Delbecq, C. J.; Hayes, W.; Yuster, P. H. *Phys. Rev.* **1961**, *121*, 1043−1050.
(56) Matheson, M. S.; Mulac, W. A.; Rabani, J. *J. Phys. Chem.* **1963**, *67*, 2613−2617.
(57) Anbar, M.; Thomas, J. K. *J. Phys. Chem.* **1964**, *68*, 3829−3835.
(58) Langmuir, M. E.; Hayon, E. *J. Phys. Chem.* **1967**, *71*, 3808−3814.
(59) Devonshire, R.; Weiss, J. J. *J. Phys. Chem.* **1968**, *72*, 3815−3820.
(60) Jayson, G. G.; Parsons, B. J.; Swallow, A. J. *J. Chem. Soc., Faraday Trans. I* **1973**, *69*, 1597−1607.
(61) Thornton, A. T.; Laurence, G. S. *J. Chem. Soc., Dalton Trans.* **1973**, *8*, 804−813.
(62) Woods, R. J.; Lesigne, B.; Giles, L.; Ferradini, C.; Pucheault, J. *J. Phys. Chem.* **1975**, *79*, 2700−2704.
(63) Treinin, A.; Hayon, E. *J. Am. Chem. Soc.* **1975**, *97*, 1716−1721.
(64) Bisby, R. H.; Cundall, R. B.; Davies, A. K. *J. Photochem. Photobiol. A: Chem.* **1978**, *28*, 825−837.
(65) Nagarajan, V.; Fessenden, R. W. *J. Phys. Chem.* **1985**, *89*, 2330−2335.
(66) Lierse, C.; Sullivan, J. C.; Schmidt, K. H. *Inorg. Chem.* **1987**, *26*, 1408−1410.
(67) Feliz, M.; Ferraudi, G. *Inorg. Chem.* **1989**, *28*, 4422−4425.
(68) Champagne, M. H.; Mullins, M. W.; Colson, A.-O.; Sevilla, M. D. *J. Phys. Chem.* **1991**, *95*, 6487−6493.
(69) Bielski, B. H. J. *Radiat. Phys. Chem.* **1993**, *41*, 527−530.
(70) Mohan, H.; Maity, D. K.; Mittal, J. P. *J. Chem. Soc., Faraday Trans.* **1993**, *89*, 477−483.
(71) Adams, D. J.; Barlow, S.; Buxton, G. V.; Malone, T. N.; Salmon, G. A. *J. Chem. Soc., Faraday Trans. I* **1995**, *91*, 3303−3305.
(72) Buxton, G. V.; Bydder, M.; Salmon, G. A. *J. Chem. Soc., Faraday Trans. I* **1998**, *94*, 653−657.
(73) Jacobi, H.-W.; Wicktor, F.; Herrmann, H.; Zellner, R. *Int. J. Chem. Kinet.* **1999**, *31*, 169−181.
(74) Sherrill, M. S.; Izard, E. F. *J. Am. Chem. Soc.* **1931**, *53*, 1667−1674.
(75) Thornton, A. T.; Laurence, G. S. *J. Chem. Soc., Dalton Trans.* **1973**, 1632−1636.
(76) Wang, T.; Kelly, M. D.; Cooper, J. N.; Beckwith, R. C.; Margerum, D. W. *Inorg. Chem.* **1994**, *33*, 5872−5878.
(77) Huie, R. E. Private communication.
(78) Thomas, J. K. *J. Phys. Chem.* **1963**, *67*, 2593−2595.
(79) Wu, D.; Wong, D.; Bartolo, B. D. *J. Photochem.* **1980**, *14*, 303−310.
(80) Kläning, U. K.; Sehested, K.; Holcman, J. *J. Phys. Chem.* **1985**, *89*, 760−763.
(81) Jacobi, H.-W.; Herrmann, H.; Zellner, R. *Ber. Bunsen-Ges. Phys. Chem.* **1997**, *101*, 1909−1913.
(82) Wagner, I.; Karthäuser, J.; Strehlow, H. *Ber. Bunsen-Ges. Phys. Chem.* **1986**, *90*, 861−867.
(83) Yu, X.-Y. Kinetics of Free Radical Reactions Generated by Laser Flash Photolysis of OH + Cl^- and SO_4^- + Cl^- in the Aqueous Phase−Chemical Mechanism, Kinetics Data and Their Implications. Ph.D. Thesis (Chemistry), The University of Michigan, Ann Arbor, MI, 2001.
(84) de Violet, P. F. *Rev. Chem. Intermediates* **1981**, *4*, 121−169.
(85) Wicktor, F.; Donati, A.; Herrmann, H.; Zellner, R. *Phys. Chem. Chem. Phys.* **2003**, *5*, 2562−2572.
(86) White, J. U. *J. Opt. Soc. Am.* **1942**, *32*, 285.
(87) Synergy. *KaleidaGraph*, 3.51 ed.; Synergy Software: Reading, PA, 2001.
(88) Press, W. H.; Teukolsky, S. A.; Vetterling, W. T.; Flannery, B. P. Levenberg−Marquardt Method. *Numerical Recipes in FORTRAN The Art of Scientific Computing*, 2nd ed.; Cambridge University Press: New York, 1992; Vol. 1, pp 678−683.
(89) Kim, K.-J.; Hamill, W. H. *J. Phys. Chem.* **1976**, *80*, 2320−2325.
(90) Livinston, J.; Morgan, R.; Crist, R. H. *J. Am. Chem. Soc.* **1927**, *49*, 338−346.
(91) Poskrebyshev, G. A.; Huie, R. E.; Neta, P. *J. Phys. Chem. A* **2003**, *107*, 1964−1970.
(92) Wine, P. H. Private communication.
(93) Gilbert, B. C.; Stell, J. K.; Peet, W. J.; Radford, K. J. *J. Chem. Soc., Faraday Trans. I* **1988**, *84*, 3319−3330.
(94) Henbest, K.; Douglas, P.; Garley, M. S.; Mills, A. *J. Photochem. Photobiol. A: Chem.* **1994**, *80*, 299−305.
(95) Jacobi, H.-W.; Herrmann, H.; Zellner, R. Kinetic investigation of the Cl_2^- radical in the aqueous phase. In *Homogeneous and heterogeneous chemical processes in the troposphere*; Mirabel, P., Ed.; European Commission: Luxembourg, Belgium, 1996; pp 172−176.
(96) Kläning, U. K.; Wolff, T. *Ber. Bunsen-Ges. Phys. Chem.* **1985**, *89*, 243−245.
(97) Steinfeld, J. I.; Francisco, J. S.; Hase, W. L. Complex Reactions. *Chemical Kinetics and Dynamics*, 2nd ed.; Prentice-Hall, Inc.: Upper Saddle River, NJ, 1989; Chapter 2, pp 21−108.
(98) Steinfeld, J. I.; Francisco, J. S.; Hase, W. L. Reaction in solution. In *Chemical Kinetics and Dynamics*, 2nd ed.; Prentice-Hall, Inc.: Upper Saddle River, NJ, 1989; Chapter 4, pp 156−178.
(99) See ref 83.
(100) Ward, J. F.; Kuo, I. Steady state and pulse radiolysis of aqueous chloride solutions of nucleic acid components. An international conference sponsored by Argonne National Laboratory: Argonne, IL, 1968.
(101) Patterson, L. K.; Bansal, K. M.; Bogan, G.; Infanta, G. A.; Fendler, E. J.; Fendler, J. H. *J. Am. Chem. Soc.* **1972**, *94*, 9028−9032.
(102) Zhestkova, T. P.; Pikaev, A. K. *Bull. Akad. Nauk SSSR, Div. Chem. Sci.* **1974**, *23*, 877−878.
(103) Broszkiewicz, R. K. *Bull. Acad. Pol. Sci., Ser. Sci. Chim.* **1976**, *XXIV*, 123−131.
(104) Zansokhova, A. A.; Kabakchi, S. A.; Pikaev, A. K. *High Energy Chem.* **1977**, *11*, 50−54.
(105) Navaratnam, S.; Parsons, B. J.; Swallow, A. J. *Radiat. Phys. Chem.* **1980**, *15*, 159−161.
(106) Gogolev, A. Y.; Makarov, I. E.; Pikaev, A. K. *High Energy Chem.* **1984**, *18*, 390−398.
(107) Debye, P.; Hückel, E. *Phys. Z.* **1923**, *24*, 185.
(108) Brönsted, J. N.; Livingston, R. *J. Am. Chem. Soc* **1927**, *49*, 435−446.
(109) Davies, C. W. *Prog. React. Kinet.* **1961**, *1*, 161−186.
(110) Davies, C. W. *Ion Association*; Butterworths: Washington, DC, 1962.
(111) Buxton, G. V.; Bydder, M.; Salmon, G. A.; Williams, J. E. *Phys. Chem. Chem. Phys.* **2000**, *2*, 237−245.
(112) Alegre, M. L.; Gerones, M.; Rosso, J. A.; Bertolotti, S. G.; Braun, A. M.; Martire, D. O.; Gonzalez, M. C. *J. Phys. Chem. A* **2000**, *104*, 3117−3125.
(113) Lesigne, B.; Ferradini, C.; Pucheault, J. *J. Phys. Chem.* **1973**, *77*, 2156−2158.
(114) Herrmann, H.; Reese, A.; Zellner, R. *J. Mol. Struct.* **1995**, *348*, 183−186.
(115) Chitose, N.; Katsumura, Y.; Domae, M.; Zuo, Z.; Murakami, T. *Radiat. Phys. Chem.* **1999**, *54*, 385−391.
(116) Ziajka, J.; Warneck, P. *EUROTRAC Symposium '93*; Borrell, P. M., Borrell, P., Cvitas, T., Kelly, K., Seiler, W., Eds.; Computational Mechanics Publications: Southhampton, U.K., 1993.
(117) Zumdahl, S. S. Acids and Bases. In *Chemistry Instructor's Edition*, 3rd ed.; Houghton-Mifflin: Boston, 1993; Chapter 14, p 642.
(118) Gilbert, C. W.; Ingalls, R. B.; Swallow, A. J. *Radiat. Phys. Chem.* **1977**, *10*, 221−225.
(119) Bjergbrakke, E.; Navaratnam, S.; Parsons, B. J.; Swallow, A. J. *Radiat. Phys. Chem.* **1987**, *30*, 59−62.
(120) Devonshire, R.; Weiss, J. J. *J. Phys. Chem.* **1968**, *72*, 3815.
(121) Zehavi, D.; Rabani, J. *J. Phys. Chem.* **1972**, *76*, 312−319.
(122) Schuchmann, H.; Deeble, D. J.; Olbrich, G.; von Sonntag, C. *Int. J. Radiat. Biol.* **1987**, *51*, 441.
(123) Jacobs, D. A. H. *The State of the Art in Numerical Analysis*; Academic Press: New York, 1977.
(124) Subhani, M. S.; Kauser, Z. *Rev. Roum. Chim.* **1978**, *23*, 1129.